A stochastic structural stability theory model of the drift wave–zonal flow system

Brian F. Farrell[1,a)] and Petros J. Ioannou[2,b)]
[1]*Department of Earth and Planetary Sciences, Harvard University, 24 Oxford Street, Cambridge, Massachusetts 02138, USA*
[2]*Department of Physics, University of Athens, Panepistimiopolis, Zografos 15784, Greece*

(Received 7 August 2009; accepted 12 October 2009; published online 30 November 2009)

A remarkable phenomenon in turbulent flows is the spontaneous emergence of coherent large spatial scale zonal jets. In this work a comprehensive theory for the interaction of jets with turbulence, stochastic structural stability theory, is applied to the problem of understanding the formation and maintenance of the zonal jets that are crucial for enhancing plasma confinement in fusion devices. © *2009 American Institute of Physics*. [doi:10.1063/1.3258666]

I. INTRODUCTION

Zonal flows arising spontaneously from drift wave turbulence play an important role in enhancing plasma confinement in fusion devices. Despite the practical and theoretical importance of obtaining a predictive understanding of this phenomenon, a comprehensive theory for the dynamics of jets emergent from plasma turbulence has been lacking. By a comprehensive theory is understood an analytic system derived from the equations governing the plasma dynamics that predicts both jet formation from small initial perturbations and jet equilibration at finite amplitude together with the structure of both the jets and the turbulence that supports the jets. In this work such a comprehensive theory based on the methods of stochastic structural stability theory (SSST) is described and applied to the coupled drift wave–zonal flow (DW-ZF) system. This theory provides new prescriptive strategies for manipulating and controlling the DW-ZF state.

Current theoretical understanding of DW-ZF dynamics is based in part on analogy between the observed jet/turbulence interaction and the behavior of solutions to the predator-prey model. This analogy is founded on statistical random wave theory and captures the essence of the instability/equilibration process as well as the existence of limit cycles and chaotic states. A correct physical theory must explain this observed behavior and comport with the essential results of random wave theory, but the predator-prey model is not itself a solution of the equations and so cannot by itself be accepted as a comprehensive theory. The modulational instability is invoked to account for the initial jet formation and this theory captures the essence of the turbulence/jet interaction but does not address equilibration and therefore cannot be considered a comprehensive theory. These concepts are extensively reviewed by Diamond *et al.*[1]

The phenomenon of spontaneous jet formation from turbulence is quite general and coherent jets that are not forced at the jet scale are often observed in turbulent flows with a familiar geophysical example being the zonal winds of the gaseous planets.[2] This phenomenon of spontaneous jet formation in turbulence has been extensively investigated in observational and theoretical studies[1,3–10] as well as in laboratory experiments.[11–17] The mechanism by which these zonal flows form and are maintained is systematic organization of upgradient eddy momentum flux in which the transfer of momentum occurs directly from the eddy field to the zonal flow without passing through intermediate scales, in contrast to the prediction of theories based on two dimensional (2D) turbulence cascades.[1,7,18–21]

In the DW-ZF system the drift wave perturbations arise from the internal instability of the imposed density gradient, from sources external to the intrinsic dynamics of the drift waves and at a given scale from transfer between scales by the internal quadratic nonlinear advection. Because these processes produce perturbations with short time and space scales compared to the time and space scale of the jet, the associated eddy dynamics can be simulated using a stochastic turbulence model (STM) in which the nonlinear scattering and extrinsic excitation are modeled as stochastic.[22–27] The STM provides an analytic method to obtain the dynamics of the quadratic statistics of a turbulent eddy field associated with a given jet structure. Coupling a time dependent STM to an evolution equation for the jet produces a dynamical system for the coevolution of the jet and the self-consistent quadratic statistics of its associated turbulence; this is the method of SSST. The SSST system can be interpreted as the dynamics of the ensemble mean jet and the ensemble mean associated turbulence in which the turbulence is modeled by the ensemble mean perturbation linear dynamics with a stochastic approximation for the nonlinear dynamics. The solution for the eddy field is in terms of a covariance matrix from which can be obtained the Gaussian probability density function approximation for the variance and quadratic fluxes of the turbulence. The solution trajectory of the SSST equations often converges to a fixed point state of balance between the turbulence and the jet; however, limit cycles and chaotic solutions also occur.[8,9,28–30] Chaotic trajectories of the SSST system correspond not to chaos of an individual turbulent state trajectory, which typically would be associated with a fixed point of the SSST system, but rather to chaos of the zonal mean of the turbulent state. A familiar example of the

a)Electronic mail: farrell@seas.harvard.edu.
b)Electronic mail: pjioannou@phys.uoa.gr.

manifestation of this chaos is the irregular bursting behavior seen in drift wave turbulence.[16]

An equilibrium state of balance between a zonal flow and its associated field of drift wave turbulence requires that the momentum flux divergence arising from the turbulence precisely balance the zonal flow momentum loss to friction, if any. The requirement of a precise balance between zonal flow forcing and dissipation, if any, is far more demanding than that the shear associated with the jet simply suppress the turbulence while the turbulence produces upgradient momentum flux. The remarkable fact is that the turbulence, which depends on the zonal flow, and the zonal flow, which depends on the turbulence, mutually adjust to produce balanced states. Having the SSST analytic dynamics of the DW-ZF system allows us to predict parameter values for which robust equilibrium DW-ZF regimes are maintained, to predict parameter values for which time dependent periodic and chaotic DW-ZF regimes occur, to predict transition between these regimes when two regimes exist at the same parameter values, and ultimately to predict the breakdown of the zonal flow regime.

Closer inspection of the density transport mechanism reveals that the observed and simulated DW-ZF equilibrium jet density transport suppression cannot be understood using the concept of effective diffusion.[31] In effective diffusion theory it is assumed that transport of a passive scalar is proportional to the scalar gradient with coefficient $D_{\mathrm{eff}}=vl$ in which v and l are the characteristic velocity and spatial correlation scales of the turbulence. Transport can vary either due to changes in the characteristic velocity or in the eddy correlation scale. In this work we solve for the correlation between velocity and density fluctuations directly revealing turbulent transport both up and down the mean gradient, in agreement with observations and simulations,[17,32] and implying that the density transport process in drift wave turbulence is not diffusive in nature. Instead we find that large scale coherent structures rather than small scale eddy diffusion are responsible for density transport.[33]

Closer inspection of the dynamics of the interaction between perturbations and zonal flows reveals that understanding reduction in turbulence variance by zonal flows through the concept of shear suppression by zonal flow advection is incomplete. Shear suppression has roots in Wentzel–Kramers–Brillouin theory and the concept of a continuous spectrum of advected harmonic waves. However, to properly understand perturbation dynamics in jets a full wave solution must be obtained because the perturbation dynamics supports a complete set of large scale coherent modes that are, in general, not orthogonal and among which exists a subset that is potentially unstable. Interaction between the zonal jet and the eddy field systematically stabilizes these modes[34–36] during the establishment of a statistical equilibrium. Moreover, the non-normal equilibrium jet dynamics supports a subset of stable structures that produce robust growth under internally and externally imposed excitations. These stochastic optimal (SO) perturbations[23] comprise a small subset of structures but these are the structures responsible for growth of perturbations due to interaction with the zonal shear and density gradient. Using SSST we solve for the complete normal mode eigenstructure of the equilibrium jet as well as the SO and empirical orthogonal function (EOF) (Karhunen–Loeve) decomposition of the ensemble mean turbulence variance and cross variance in the velocity and density fields. This analysis provides full information on the structure and dynamics of the perturbations responsible for producing the turbulence variance and fluxes.

The mechanism of jet formation in plasmas can be studied for turbulence arising from external, internal, or a combination of sources. The Charney–Hasegawa–Mima equation provides the simplest model system as it uses only external turbulence excitation. Zonal jet formation in this model is identical to that in the equivalent barotropic vorticity equation.[9] However, because in the DW-ZF problem there exists an internal instability associated with the density gradient this problem is more comprehensively modeled using the modified Hasegawa–Wakatani (HW) equations which govern plasma dynamics in a 2D slab model. These equations are similar, although not identical, to the baroclinic two-layer model.[28] In this work we use the HW equations to study DW-ZF dynamics.

The SSST equations incorporate a STM but these equations are themselves deterministic and autonomous with dependent variables the zonal flow and the ensemble mean covariance of the turbulence. It follows that the perspective on stability provided by these equations differs from the more familiar perspective based on the perturbation stability of the zonal flow. In fact, the primary bifurcation in these equations has no counterpart in zonal flow stability analysis; it is rather a cooperative instability in which the perturbation zonal flow organizes the background turbulence to produce flux divergences configured to amplify the jet leading to an emergent turbulence-zonal flow instability that need not coincide with perturbation instability of the jet. The SSST equations approximate the nonlinear zonal mean dynamics for the DW-ZF flow system and this system in many cases supports equilibration of the emergent jets and their consistent turbulence fields at finite amplitude. These finite amplitude equilibria in turn lose structural stability as a function of parameters and this instability is associated either with bifurcation to another equilibrium or with loss of a stable equilibrium state. While it is true that loss of modal jet stability by an equilibrium state as a function of a parameter also implies loss of structural stability, the converse is not true. For this reason bounds on zonal jet amplitude based on modal instability of the jet are not tight and can often be improved by analysis of the structural stability of the jet.

A gradient driven flow with constant density gradient is assumed in the examples below for simplicity although the particle flux is calculated and could be used with an appropriate density gradient forcing parametrization to obtain equilibria in which the density gradient participates in the equilibration. However, as equilibrium is approached the fluxes are typically suppressed implying long time scales for changes in the equilibrium density gradient by flux divergence and the likelihood that external driving mechanisms dominate density gradient variation.

II. FORMULATION

A. The HW drift wave turbulence equations

We use the modified HW equations.[37] These equations model the turbulence of the edge region of a tokamak plasma with fractional density decreasing in the radial direction x at a constant rate κ, so that $n(x)=n_0 e^{-\kappa x}$, and in a constant background magnetic field $\mathbf{B}=B_o\hat{\mathbf{z}}$ in the toroidal z direction. The HW equations govern the dynamics of the electrostatic potential $e\phi/T_e$ and the ion density n/n_0 in a Cartesian approximation of the radial-poloidal, x-y, plane.

The ion vorticity, $\zeta=\Delta\phi$, and the density fluctuations n solve following Numata *et al.*:[37]

$$\partial_t \zeta + J[\phi,\zeta] = \alpha(\phi' - n') + \nu\Delta\zeta, \tag{1a}$$

$$\partial_t n + J[\phi,n] = \alpha(\phi' - n') - \kappa\partial_y\phi + \nu\Delta\zeta, \tag{1b}$$

with Jacobian $J[f,g]\equiv(\partial_x f)(\partial_y g)-(\partial_y f)(\partial_x g)$. The fields are decomposed into zonal means and departures from zonal means,

$$\phi = \bar{\phi} + \phi', \quad n = \bar{n} + n', \tag{2}$$

with the zonal mean, denoted by a bar, defined as the mean in the poloidal direction y,

$$\bar{f} = L_y^{-1}\int_0^{L_y} f(x,y,t)dy. \tag{3}$$

The flow velocities are

$$u = -\partial_y\phi, \quad v = \partial_x\phi. \tag{4}$$

The parameter α controls the strength of the electron resistivity that couples the electrostatic field with the ion density perturbations. For $\alpha=0$ Eq. (1a) corresponds to the hydrodynamic 2D vorticity equation while Eq. (1b) corresponds to the advection-diffusion of n' as a passive scalar in the presence of a mean fractional radial density gradient $-\kappa$. In the limit $\alpha\to\infty$ the density and electrostatic field couple rigidly and obey the Charney–Hasegawa–Mima equation.[38] The dynamics of this equation, which governs the formation of zonal flows in both the geophysical and the plasma context, has been studied in recent theoretical work on zonal flow generation.[3,8–10] Hereafter, we treat the more general quasiadiabatic case with $\alpha=1$ and allow for instability by including an ion density gradient κ, which will be treated as a variable parameter.

In the nondimensionalization of the equations lengths are scaled by the Larmor radius $\rho_s=\sqrt{T_e/m_i\omega_{ci}^{-1}}$ and time by the electron cyclotron frequency $\omega_{ci}=eB_0/m_i$. A typical Larmor radius, $\rho_s=1$ mm, is obtained for a magnetic field of 1 T and electron temperature $T_e=95.6$ eV; also for these values $\omega_{ci}^{-1}=10^{-8}$ s/rad and the corresponding velocity scale $\rho_s\omega_{ci}$ is 95.6 km/s. The channel is taken doubly periodic in both x and y.

The zonal average of Eq. (1a) gives the equation for the zonal jet,

$$\partial_t\bar{v} = -\overline{u'\zeta'} - r_m\bar{v}, \tag{5}$$

where $\bar{v}=D\bar{\phi}$ and $D\equiv\partial_x$. The zonal flow is damped linearly at the mean collisional damping rate r_m, which will typically be taken to be $r_m=10^{-4}$ although we will also present results in the collisionless limit, $r_m=0$

The nonzonal components obey the equations

$$\partial_t\zeta' = -\bar{v}\partial_y\zeta' + (D^2\bar{v})\partial_y\phi' + \alpha(\phi'-n') + \nu\Delta\zeta' + F(\zeta'), \tag{6a}$$

$$\partial_t n' = -\bar{v}\partial_y n' - \kappa\partial_y\phi' + \alpha(\phi'-n') + \nu\Delta n' + F(n'), \tag{6b}$$

with nonlinear scattering term,

$$F(f) = -\partial_x(u'f' - \overline{u'f'}) - \partial_y(v'f' - \overline{v'f'}). \tag{7}$$

These equations can sustain turbulence without external forcing due to the radial density flux, $\overline{u'n'}$, in the presence of the mean density gradient.[37] We now briefly review the energetics of these equations. The total energy E is the sum of the zonal mean kinetic energy,

$$\bar{E} = \frac{1}{2}\int_0^{L_x}\bar{v}^2 dx, \tag{8}$$

and the eddy energy,

$$E' = \frac{1}{2}\int_0^{L_x}(|\nabla\phi'|^2 + n'^2)dx. \tag{9}$$

From the zonal mean Eq. (5) we obtain

$$\frac{d\bar{E}}{dt} = \Gamma_e - 2r_m\bar{E}, \tag{10}$$

where

$$\Gamma_e = -\int_0^{L_x}\bar{v}\overline{u'\zeta'}dx \tag{11}$$

is the time rate of change of the zonal mean energy due to the eddy induced mean zonal acceleration $-\overline{u'\zeta'}$. Similarly, we obtain from the perturbation equations (6a) and (6b)

$$\frac{dE'}{dt} = -\Gamma_e + \Gamma_n - \Gamma_\alpha - \Gamma_\nu + F, \tag{12}$$

where

$$\Gamma_n = \kappa\int_0^{L_x}\overline{u'n'}dx \tag{13}$$

is the rate of perturbation energy gain due to perturbation density flux down the mean density gradient. This term provides the internal energy source for the turbulence. The term

$$\Gamma_\alpha = \alpha\int_0^{L_y}(\phi'-n')^2 dx, \tag{14}$$

corresponding to resistive coupling, is always dissipative as is the diffusion,

$$\Gamma_\nu = \int_0^{L_y} (|\nabla \zeta'|^2 + |\nabla n'|^2) dx. \quad (15)$$

The term F is the rate of energy input by external excitation. This external energy input rate is constant if the excitation is delta correlated and state independent.

B. The SSST system governing DW-ZF dynamics

We parametrize the nonlinear scattering term (7) in the eddy equations (6a) and (6b) by stochastic forcing, which is the STM closure.[39,40] The STM accurately simulates both the structure of the eddy field and of the quadratic fluxes in shear turbulence including that of the Earth's atmosphere, which is a particularly well observed turbulent medium.[26,27,41–43]

We represent the perturbation fields using Fourier components in the poloidal direction y,

$$\phi' = \sum_k \hat{\phi}_k(x,t) e^{iky}, \quad n' = \sum_k \hat{n}_k(x,t) e^{iky}, \quad (16)$$

and discretize the equations in the radial direction x, so that the state $\psi_k = [\hat{\phi}_k, \hat{n}_k]^T$ is prescribed by the values, for each Fourier component, of the electrostatic potential and the perturbation density on an equally spaced grid. Under the simplifying assumption that the stochastic forcing has sufficiently short temporal correlation that it can be approximated as white noise, the second moment statistics of the fluctuating field ψ_k are fully described by the covariance matrix $\mathbf{C}_k = \langle \psi_k \psi_k^\dagger \rangle$ ($\langle \cdot \rangle$ denotes ensemble averaging) which evolves according to the deterministic Lyapunov equation,

$$\frac{d\mathbf{C}_k}{dt} = \mathbf{A}_k(\bar{v})\mathbf{C}_k + \mathbf{C}_k \mathbf{A}_k^\dagger(\bar{v}) + \mathbf{Q}_k, \quad (17)$$

in which $\mathbf{Q}_k$ is the covariance representing the ensemble average distribution of the stochastic forcing in the radial direction[23] and $\mathbf{A}_k(\bar{v})$ is the linear operator in Eqs. (6a) and (6b) which depends affinely on the zonal flow $\bar{v}(x,t)$. The operator $\mathbf{A}_k$ in Eq. (17) in matrix form is

$$\mathbf{A}_k = \begin{pmatrix} \Delta_k^{-1}[-ik\,\mathrm{diag}(\bar{v})\Delta_k + ik\,\mathrm{diag}(D^2\bar{v}) + \alpha\mathbf{I} + \nu\Delta_k^2] & -\alpha\Delta_k^{-1} \\ (-ik\kappa + \alpha)\mathbf{I} & -ik\,\mathrm{diag}(\bar{v}) - \alpha\mathbf{I} + \nu\Delta_k \end{pmatrix}, \quad (18)$$

in which $\mathbf{I}$ is the identity, $\mathrm{diag}(\bar{v})$ is the diagonal matrix with the diagonal element values $\bar{v}$ at the grid points, $\Delta_k = D^2 - k^2\mathbf{I}$ is the Laplacian in matrix form for wavenumber k, and Δ_k^{-1} its inverse. If $\mathbf{Q}_k$ represents scattering by the advective nonlinearity rather than external sources of excitation, then a dissipation can be added to the linear operators to ensure that no net energy is introduced into the system (because the nonlinear terms only redistribute energy). Also, $\mathbf{Q}_k$ can be made an appropriate function of the amplitude of the perturbation variance in order to accurately parametrize the quadratic nonlinearity of the advective Jacobian. More comprehensive closures of this sort have been used in other contexts;[30,44] however, it is sufficient for our present purposes to use the simplest parametrization in which the system is stochastically excited with state independent forcing and the behavior of the system is investigated as a function of the amplitude of this excitation.

The Lyapunov equation (17) determines $\mathbf{C}_k$ and this covariance in turn determines the ensemble mean vorticity flux,

$$\langle u' \Delta \phi' \rangle = \sum_k \frac{1}{2} \Re[-ik\langle \hat{\phi}_k \Delta_k \hat{\phi}_k'^* \rangle] = \sum_k \frac{k}{2} \Im[\mathrm{diag}(\mathbf{C}_k \Delta_k^\dagger)]. \quad (19)$$

However, it is the zonal mean vorticity flux that appears in the zonal flow equation (5) but under the ergodic assumption the zonal mean can be replaced by the ensemble mean,

$$\langle u' \Delta \phi' \rangle = \overline{u' \Delta \phi'}. \quad (20)$$

This requires that there be many independent realizations of eddy activity in the poloidal direction, and in that limit we obtain the ensemble mean equations,

$$\partial_t \bar{v} = -\sum_k \frac{k}{2} \Im[\mathrm{diag}(\mathbf{C}_k \Delta_k^\dagger)] - r_m \bar{v}, \quad (21a)$$

$$\frac{d\mathbf{C}_k}{dt} = \mathbf{A}_k(\bar{v})\mathbf{C}_k + \mathbf{C}_k \mathbf{A}_k^\dagger(\bar{v}) + \mathbf{Q}_k. \quad (21b)$$

The equation for the turbulence covariance, Eq. (21b), and the equation for the mean zonal flow, Eq. (21a), together comprise a closed nonlinear system for the evolution of the zonal flow under the influence of its consistent field of turbulent eddies. Although the effects of the ensemble mean turbulent fluxes are retained in this system, the fluctuations associated with the turbulent eddy dynamics are suppressed and the dynamics becomes autonomous and deterministic. These SSST equations can be interpreted as the dynamical equations for the evolution of a quadratic (Gaussian) approximation to the dynamics of the probability distribution of the turbulent DW-ZF system. This concept invites novel perspectives such as that of chaos of the zonal mean state of a turbulent system as distinct from chaos of a realization of the system. We show examples of zonal mean state chaos in DW-ZF turbulence below. However, the SSST system trajectory is often not chaotic but instead asymptotes to a fixed point equilibrium, and in these cases the dynamics of DW-ZF equilibria emerge with great clarity in the SSST system.

As another illustration of the insight provided by this system we note that zonal jets arise in SSST as easily analyzed linear instabilities. This jet forming instability is an example of a new class of instability in fluid dynamics; it is an emergent instability that arises essentially from the interaction between the zonal flow and the turbulence. One may think of a perturbation zonal flow organizing the surrounding turbulence to produce a momentum flux divergence that amplifies that perturbation zonal flow. The particular perturbation zonal flow structure that organizes the turbulence to exactly amplify its own structure is obtained as an eigenfunction of the perturbation SSST system linearized about a marginally stable SSST equilibrium. This instability equilibrates at finite amplitude and this finite amplitude SSST equilibrium, consisting of the zonal flow and associated consistent eddy field, can often be connected by continuation in an appropriate parameter, such as the density gradient, to nearby finite amplitude equilibrium states.

In addition to simply continued equilibria there also exist equilibria that are isolated to variation of a given parameter as, for instance, a strong zonal flow equilibrium exists at a moderate density gradient and turbulence intensity that cannot be connected by continuation starting from a weak zonal flow equilibrium at a small density gradient. However, external turbulence excitation can be used as a control parameter to promote the system to such an isolated equilibrium state. In addition to parameter control we may also perturb the zonal flow to promote the system to an isolated equilibrium state. Promoting the DW-ZF system to different regime states by parameter control is analogous to instigating a laminar/turbulent transition in shear flow turbulence where the Reynolds number is the control parameter.

C. Parameters

Unless otherwise indicated calculations were performed with 64 points in the x direction and 8 harmonics in the (y) direction comprising wavenumbers $k=[k_0,3k_0,5k_0,7k_0,9k_0,11k_0,13k_0,15k_0]$ with $k_0=0.15$ in a doubly periodic channel with $L_y=2\pi/k_0$ and $L_x=L_y/4$. The stochastic forcing is taken to have an identity covariance in vorticity corresponding to a one grid point correlation and is normalized so that the energy input by the stochastic forcing is the same for all poloidal wavenumbers. The excitation of the electrostatic field and the density field is correlated in order to facilitate the adjustment of the two fields (similar results are obtained using uncorrelated forcing). The amplitude of the stochastic forcing is given in terms of the equivalent $u_{\rm rms}$ velocity that would be maintained by the forcing with no zonal flow and with $\kappa=0$. Dissipation parameters used are $\nu=10^{-2}$, $\alpha=1$, and $0\leqslant r_m\leqslant 10^{-4}$.

III. DW-ZF BEHAVIOR IN PARTICULAR REGIMES OF DYNAMICAL INTEREST

A. Formation of zonal jets starting from a nonequilibrium state

The starting point for a systematic investigation of DW-ZF dynamics is the nonlinear SSST system initiated in a state lying on its attractor. However, the system is commonly thought of as being initiated far from its attractor in a state of high turbulence intensity but without the corresponding finite amplitude equilibrium jet. There then ensues a rapid adjustment process in which the system builds a jet corresponding to the turbulence and in the process places the system on the SSST attractor. In order to study this adjustment process consider the example of the turbulence field associated with a single poloidal wavenumber in equilibrium with a strong stochastic excitation but without its consistent zonal jet. The turbulence field is that obtained from the stochastically excited STM but without coupling to the zonal flow equation. If the zonal flow equation is coupled to the STM at this point to form the interactive SSST system, there ensues rapid formation of a consistent zonal jet. We show this rapid development of a jet from a strong initial turbulent field at the single poloidal wavenumber $m=5$ in Fig. 1 for $\kappa=0$ and no stochastic excitation. We also show the unstable case with $\kappa=1$ and in both cases the development of the zonal jet is rapid because of the feedback between the eddies and the growing zonal jet. If as an experiment the eddies are required to develop on a fixed jet structure that is not continuously modified by their dynamics then the resulting fluxes build the jet much more slowly revealing that rapid jet formation is due to the cooperative DW-ZF interaction. The build up of the jet and the concurrent suppression of the eddy energy occur due to shearing of the eddy field by the jet, a process discussed by Diamond *et al.*[1] and that is seen both in simulations[37] and observations. Because the eddy momentum flux is upgradient and increases with both the shear[29,45] and the variance, an exponential or faster growth of shear with time occurs.

Similar development occurs when there is stochastic forcing, and as a result the turbulence has a full spectrum. An example with $\kappa=1$ of jet emergence from small amplitude random initial conditions in an unstable flow with substantial stochastic excitation is shown in Fig. 2 and the process of its approach to equilibrium is shown in Fig. 3. The eddy induced zonal acceleration reaches its peak during this initial development [cf. Fig. 2(d)]. The rapid suppression of the eddy variance [cf. Fig. 2(c)] is caused by energy transfer to the zonal flow and by increased dissipation Γ_α due to increased disequilibrium of the electrostatic field ϕ' and the perturbation ion density fluctuations n' [cf. the energetics equation (12)].

After the initial development of the zonal jet by the mechanism of antidiffusive shear momentum transport as described above there follows a period of adjustment in which the SSST system attempts to stabilize the zonal flow and to establish, if the parameters allow it, a steady state equilibrium corresponding to a fixed point of the SSST equations.

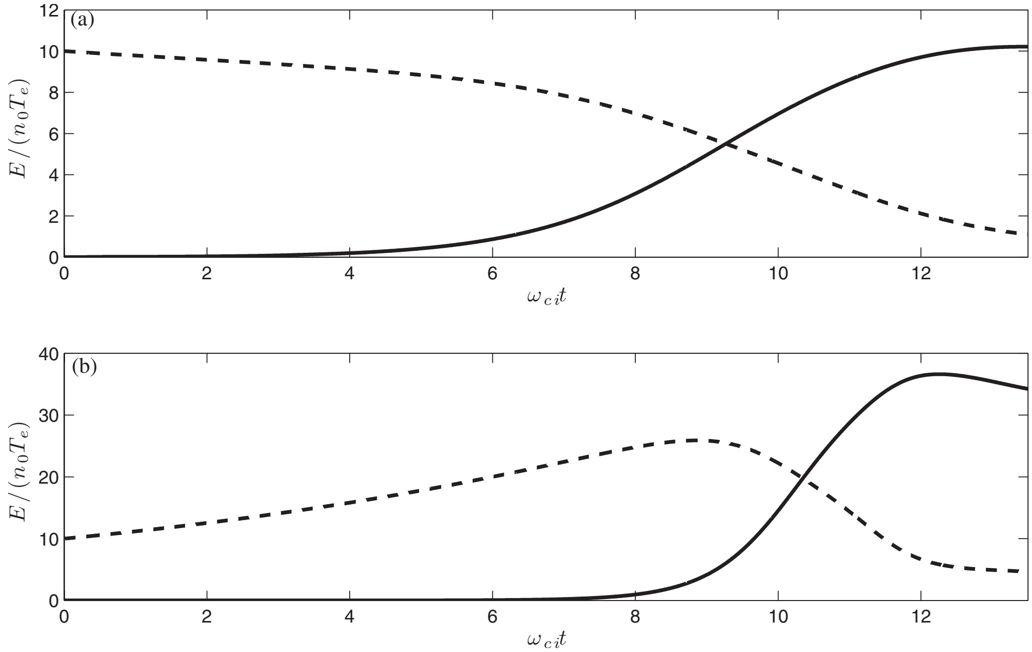

FIG. 1. Initial jet formation by the rapid adjustment process starting from a state of strong turbulence for the cases (a) $\kappa=0$ (no instability) and (b) $\kappa=1$ (strong instability). Shown are eddy kinetic energy (dashed line) and mean zonal kinetic energy (solid line) as a function of time. The eddy field is limited to poloidal wavenumber $m=5$ and there is no stochastic excitation.

This stabilization process is shown in Fig. 3 as it sequentially stabilizes the perturbation operator $\mathbf{A}_k$. Let ω denote an eigenvalue of $\mathbf{A}_k$ with real part ω_r and imaginary part ω_i. In Fig. 3 the real and imaginary parts of the temporal eigenvalues of $\mathbf{A}_k$, $kc_i=\omega_r$ and $kc_r=-\omega_i$, are shown in terms of the wave phase speed c_r and growth rate ω_r indicating this suppression of instability by the evolving zonal flow jet. As the jet adjusts to equilibrium during this phase the flow is dominated by large structures and the adjustment has a full wave modal character unlike during the initial period of jet formation from a state far removed from the system attractor in which the dynamics is shear wave antidiffusion dominated being associated essentially with rapid distortion of the initial perturbation field.

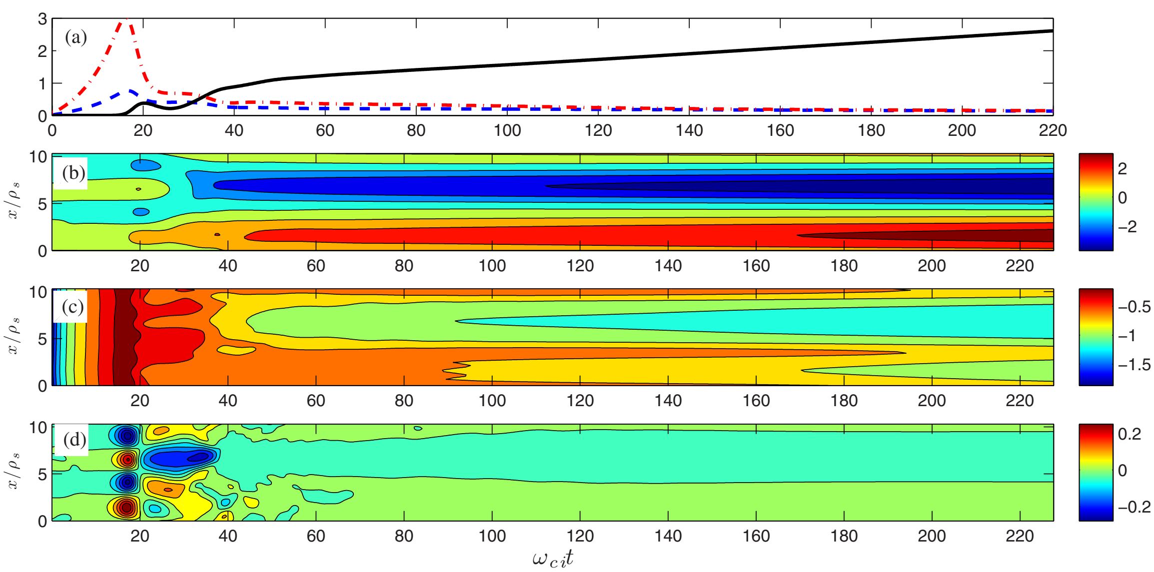

FIG. 2. (Color online) Transient development of an equilibrium zonal jet. (a) Time development of the mean kinetic energy of the zonal flow, $E_m/(n_0T_e)$ (solid line), the mean eddy kinetic energy $K_e/(n_0T_e)$ (dashed line), and the total particle flux over the channel $\Gamma_n\omega_{ci}/(n_0T_e)$ (dash-dotted line). (b) Zonal velocity $V/(\rho_s\omega_{ci})$ as a function of the radial direction and time. (c) Eddy kinetic energy, $\log_{10}[K_e/(n_0T_e)]$, as a function of the radial direction and time. (d) Eddy induced zonal flow acceleration, $-\langle u'\zeta'\rangle/(\rho_s\omega_{ci}^2)$, as a function of the radial direction and time. The parameters are $\kappa=1$, $r_m=10^{-4}\omega_{ci}$ and the stochastic excitation has equivalent rms velocity of $0.34\rho_s\omega_{ci}$.

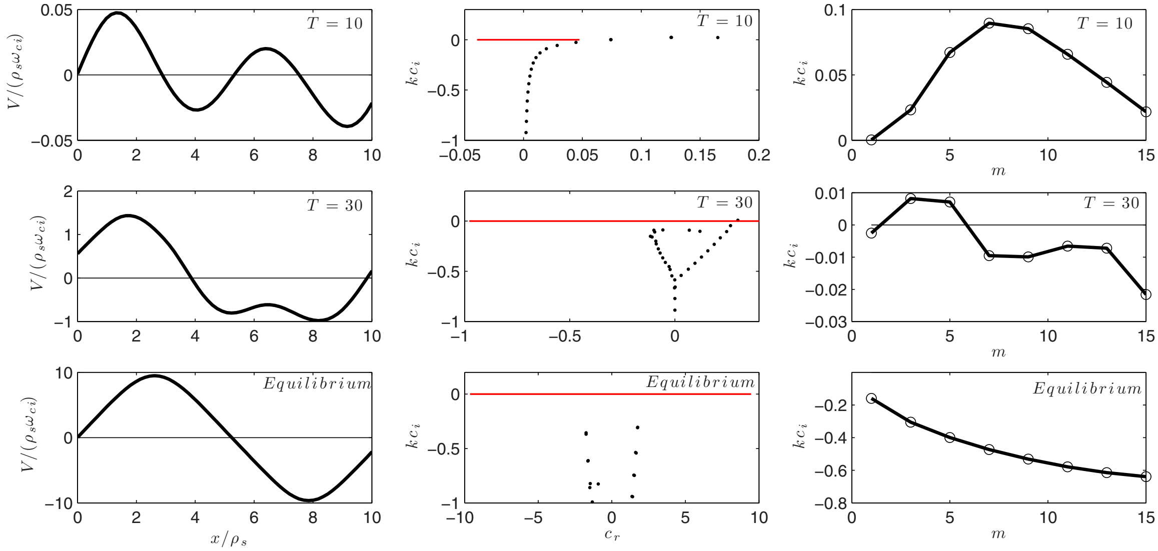

FIG. 3. (Color online) Evolution of the zonal flow and its associated spectrum for the example in Fig. 2. Left panels: zonal flow structure at $T=10,30$ and at equilibrium. Center panels: phase speed c_r and growth rate kc_i associated with the temporal eigenvalues of $\mathbf{A}_k$ for the flow in the corresponding panel for poloidal wavenumber $m=3$. The continuous line indicates the velocity interval spanned by the zonal flow. The flow is unstable when there are eigenvalues with $kc_i>0$. At equilibrium the instabilities have been stabilized. Right panels: the largest growth rate for a given poloidal wavenumber m. At equilibrium the least stable mode corresponds to the gravest poloidal wavenumber.

B. Structural instability of the zero zonal flow state as a function of the amplitude of the stochastic excitation in the absence of drift wave instability, $\kappa=0$

We turn now to dynamics on the attractor of the SSST DW-ZF system and first study the case $\kappa=0$ in which there is no drift wave instability and eddy variance is maintained solely by external excitation. In the absence of zonal flow the SSST equations (21a) and (21b) are translationally invariant in the radial direction and the vorticity flux $\overline{u'\zeta'}$ vanishes, and as a result the zero zonal flow is an equilibrium of the SSST equations for any stochastic excitation and associated turbulence level. The SSST equations can be linearized about this zero state $\bar{v}_E=0$ and the eddy covariance that corresponds to a chosen stochastic excitation of this zero state, $\mathbf{C}_{kE}$, obtained from the steady state Lyapunov equation. About this state perturbation equations can be obtained for the perturbation zonal velocity $\delta\bar{v}$ and perturbation eddy covariances $\delta\mathbf{C}_k$ in the form

$$\begin{bmatrix}\delta\bar{v}\\ \delta\mathbf{C}_k\end{bmatrix} = \mathbf{L}(\bar{v}_E,\mathbf{C}_{kE})\begin{bmatrix}\delta\bar{v}\\ \delta\mathbf{C}_k\end{bmatrix}. \tag{22}$$

The growth rate and structure of the most rapidly growing eigenmode of $\mathbf{L}$ provide insight into the mechanism of zonal jet emergence and equilibration in turbulence.[8,9] Zonal jets arise as finite amplitude nonlinear equilibria proceeding from the most rapidly growing eigenmode of $\mathbf{L}$ linearized about the zero state. Note that this jet forming instability does not, in general, coincide with loss of stability of the $\mathbf{A}_k$ operators which determine the stability of a finite amplitude zonal flow to eddy perturbation.

The SSST system can be linearized about finite amplitude SSST equilibria as well as about the zero state and the bifurcation structure about these finite equilibria can be examined as a function of parameters to determine, e.g., the circumstances under which jet breakdown occurs. It should be noted in this context that equilibria of the SSST system are necessarily perturbation stable. Consider as an example the SSST stability of the zero zonal flow state, $[\mathbf{C}_{kE},\bar{v}_E=0]$, with $\kappa=0$. In this case the zonal jet emerges as increase in stochastic excitation, $\mathbf{Q}_k$, causes the turbulence level to exceed a threshold at which point $\mathbf{L}$ becomes SSST unstable. As the amplitude of the excitation, $\mathbf{Q}_k$, is increased further this bifurcation connects to finite amplitude equilibria in which the eddies maintain finite amplitude zonal jets. The bifurcation diagram of this zonal flow as a function of excitation amplitude is shown in Figs. 4(a) and 4(c) together with the associated nonlinearly equilibrated zonal jets. For weakly supercritical excitation the structure of the zonal flow is nearly that of the most unstable mode of the $\mathbf{L}$ operator, but as the excitation increases the velocity of the zonal flow asymptotes to a constant structure as shown in Fig. 4(d).

We can understand an important aspect of the dynamics of this asymptotic structure by noting that as the stochastic excitation increases the zonal flow acceleration associated with the ensemble mean Reynolds stress divergence,

$$\langle\overline{u'\zeta'}\rangle = \frac{1}{2}\sum_k \Re(\hat{u}_k\hat{\zeta}_k^*), \tag{23}$$

is comprised of a sum of low poloidal wavenumber fluxes that decelerate the jet and high wavenumber fluxes that accelerate the jet. As excitation and turbulence level increase the vorticity flux of each component of this sum increases while the sum tends to the small residual required to balance the zonal flow dissipation because the low wavenumber downgradient and high wavenumber upgradient contributions very nearly cancel.[29] This dynamic can be seen in Fig. 5 in which the structure of the vorticity fluxes associated

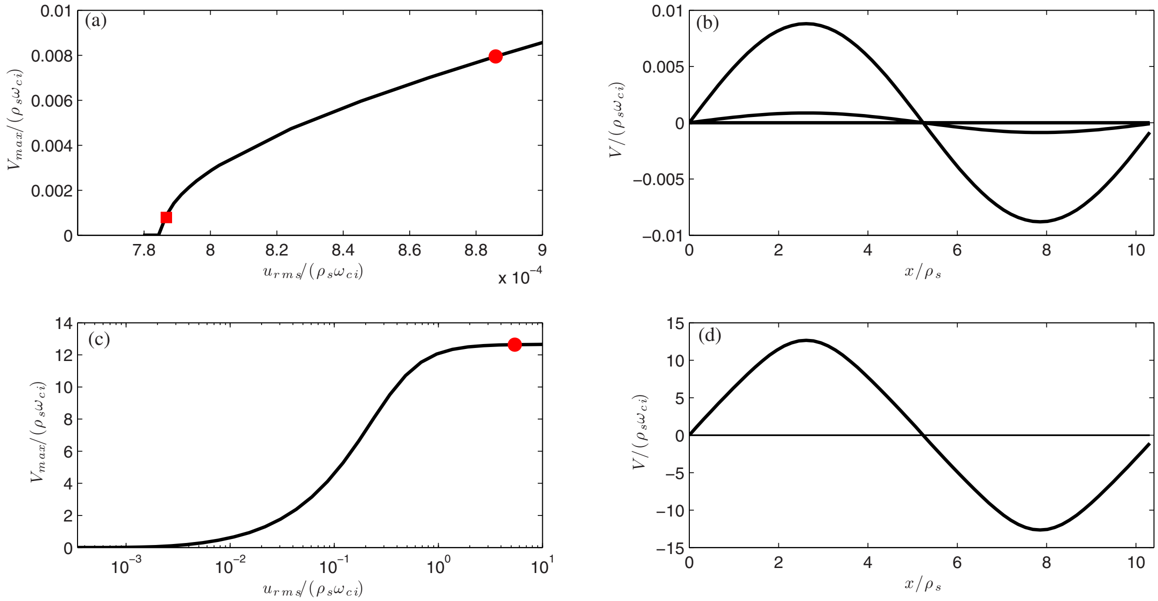

FIG. 4. (Color online) (a) Maximum zonal flow velocity as a function of stochastic excitation for $\kappa=0$. Stochastic excitation is measured by the u_{rms} that would have been maintained in the absence of a zonal flow. For the chosen parameters the critical forcing required to form zonal flows is $u_{\mathrm{rms}}=7.8\times 10^{-4}/(\rho_s\omega_{ci})$. (b) Corresponding equilibrium zonal zonal flows: the larger velocity corresponds to forcing denoted with a circle in (a), while the smaller velocity corresponds to the parameters denotes with a square in (a). (c) Continuation of the bifurcation diagram of (a) to larger forcing values. Note that as the forcing increases the maximum zonal flow velocity asymptotes to a constant. (d) The asymptotic zonal flow at large forcing. The collisional damping of the mean is $r_m=10^{-4}\omega_{ci}$.

with the equilibrium jet in Fig. 4(d) is shown. In Fig. 5(a) it is seen that wavenumbers $m=1,3,5$ oppose the jet and nearly cancel the upgradient contribution from the higher wavenumbers. This cancellation becomes all the more complete as the excitation increases and the equilibrium zonal flow assumes asymptotic form. Because the total vorticity flux vanishes in the collisionless limit, $r_m=0$, these equilibria are also the equilibria in this limit [as shown in Fig. 5(b)].

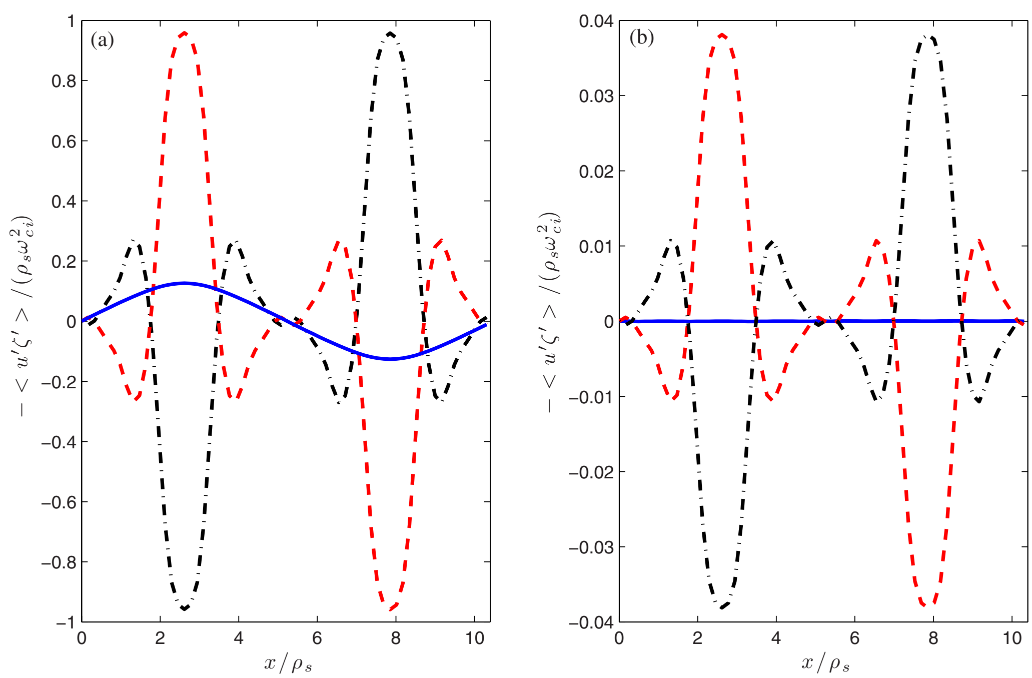

FIG. 5. (Color online) Structure of the eddy induced zonal flow acceleration $-\langle\overline{u'\zeta'}\rangle$ as a function of radius. The solid line is the total flux summed over all zonal wavenumbers multiplied by 100 (at equilibrium this is equal to $100r_m\bar{v}$). The dashed line is the acceleration induced by wavenumbers $m=7-15$. These higher waves build the zonal flow. The dash-dotted line is the acceleration induced by the small wavenumbers $m=1-5$ which tend to destroy the zonal flow. Left panel: for mean collisional damping $r_m=10^{-4}$ and the equilibrium flow in Fig. 1(d). Right panel: for $r_m=0$ (here the cancellation between downgradient and upgradient fluxes is perfect).

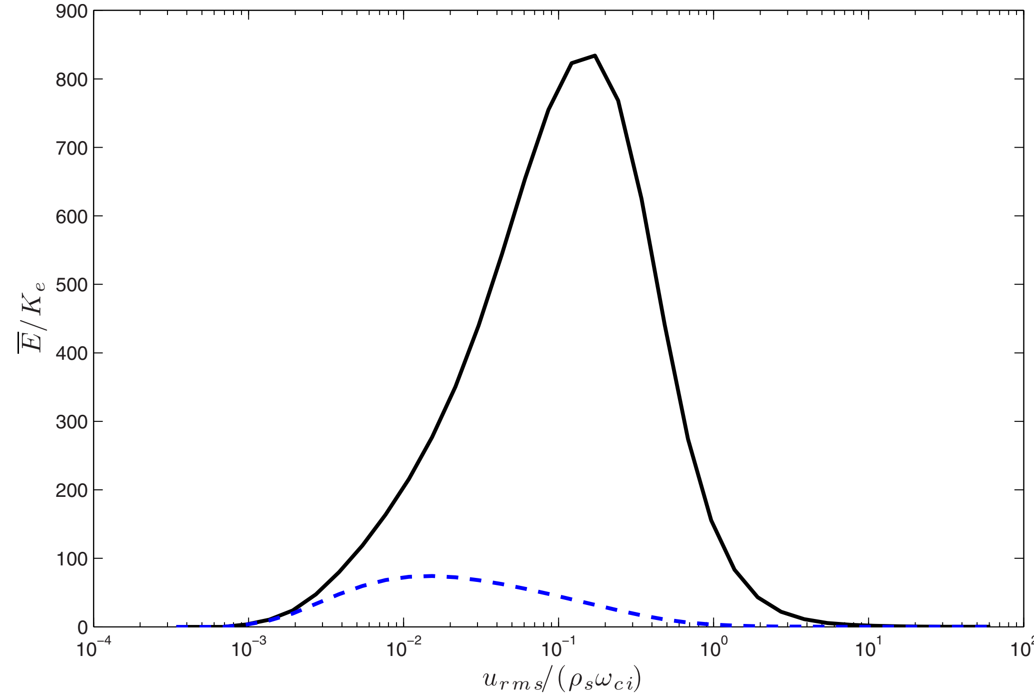

FIG. 6. (Color online) Ratio of mean zonal kinetic energy to eddy kinetic energy as a function of stochastic excitation (solid line). Ratio of the mean zonal kinetic energy to the eddy kinetic that would have been maintained in the absence of the zonal flow (dashed line). For small excitations there is no zonal flow and the ratio vanishes, also for large excitations the flow asymptotes to a constant and again the ratio vanishes. For intermediate excitations the zonal flow energy is two to three orders of magnitude larger and the turbulence energy is dominated by the zonal flow energy. The zonal flow suppresses the eddy energy by approximately an order of magnitude. For $\kappa=0$ and $r_m=10^{-4}\omega_{ci}$.

This demonstrates that in turbulence with vanishing collisional damping of the zonal flow there are nonvanishing equilibria that are independent of the turbulence intensity and have the universal structure shown in Fig. 4(d). It should be noted that while this asymptotic zonal flow does not depend on the turbulence intensity for a fixed spectrum of excitation, it is sensitive to the spectral distribution because the fluxes are upgradient for high wavenumbers and downgradient for low wavenumbers. For example, if only low wavenumbers are excited no finite equilibria result for any r_m as all fluxes oppose the jet. Conversely, if only the high wavenumbers are excited equilibria arise for $r_m \neq 0$ associated with upgradient fluxes but in this case the equilibrium zonal flow increases secularly with excitation increase until the jet became structurally unstable.

We note, in the examples shown and in agreement with observations and simulations, that the kinetic energy is concentrated in the energy of the zonal jet while the eddy kinetic energy is greatly suppressed (cf. Fig. 6).

C. Zonal flow equilibria as a function of the amplitude of stochastic excitation in the presence of drift wave instability, $\kappa>0$

Introduction of unstable density stratification $\kappa>0$ makes the zero state perturbation unstable and necessarily structurally unstable for any stochastic excitation. These unstable eddy perturbations augment the turbulence and facilitate formation of zonal jets. An example with $\kappa=1$ of jet emergence from small amplitude random initial conditions in an unstable flow with substantial stochastic excitation are shown in Figs. 2 and 3.

The radial distributions at various poloidal wavenumbers of the equilibrium particle flux and of the acceleration by the Reynolds stress are shown in Figs. 7(a) and 7(c). The eddy induced acceleration of the zonal flow by small wavenumber eddies is downgradient, opposing the jet, while the acceleration due to larger wavenumbers is upgradient, as for the case $\kappa=0$. This cancellation implies, as for the case with $\kappa=0$, that the equilibrium flow asymptotes to a fixed structure as the amplitude of the forcing increases and that this asymptotic flow is also the equilibrium flow in the collisionless limit, $r_m=0$. Similar equilibria with zero collisional damping have also been seen in turbulence simulations.[46] The asymptotic equilibrium flow shown in Fig. 8 is found to depend only weakly on κ. For $r_m=0$ this is the universal equilibrium flow for all forcing amplitudes and for all κ. However, this equilibrium is structurally unstable for large values of κ, as will be discussed.

The eddy kinetic energy peaks at the gravest poloidal scale, $m=1$. It is important to note that it is at large scales that most of the eddy energy resides and also it is the large scales that are responsible for the particle flux [the particle flux peaks for $m=3$ as shown in Fig. 7(b)] as is also found in turbulent simulations.[33] The dominance of large scales in the eddy variance and fluxes is consistent with these scales being the least damped (cf. Fig. 3), however, the eddy structure does not assume the structure of the least damped modes. We

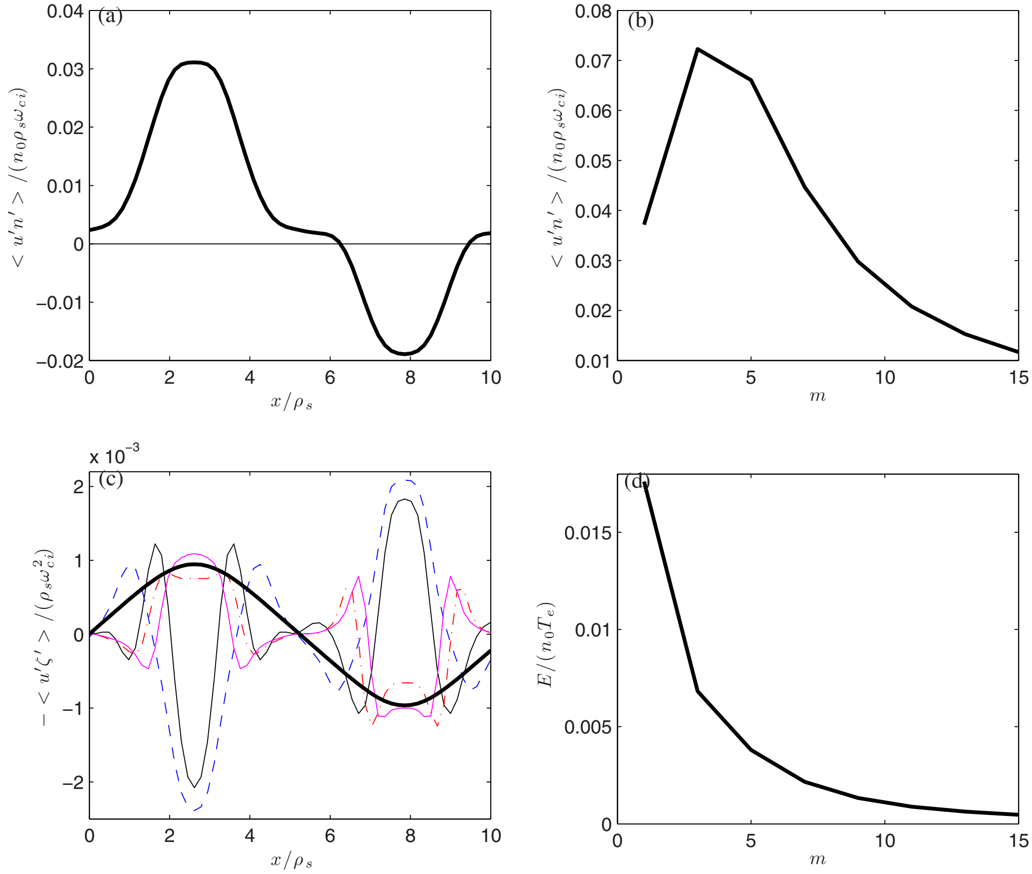

FIG. 7. (Color online) (a) Structure in radius of the particle flux at equilibrium. The particle flux is not diffusive, as it has a distinct structure and there is a region of upgradient flux that would correspond to a negative diffusion coefficient. (b) The integrated particle flux at equilibrium as a function of poloidal wavenumber m. (c) The structure of the eddy acceleration $-\langle u'\zeta'\rangle$ produced by the zonal modes. The thick solid line is the total vorticity flux which maintains the zonal flow against dissipation shown in Fig. 8. The opposing fluxes (solid and dashed lines) is the flux associated with wavenumbers $m=1,3$ while the supporting fluxes (solid and dash-dotted lines) correspond to the higher wavenumbers $m=5,7$. (d) The energy of the eddy field as a function of poloidal wavenumber. The eddy kinetic energy peaks at the gravest zonal mode $m=1$. The case is for $\kappa=1$ $r_m=10^{-4}\omega_{ci}$ and stochastic excitation equivalent to rms velocity of $0.34\rho_s\omega_{ci}$.

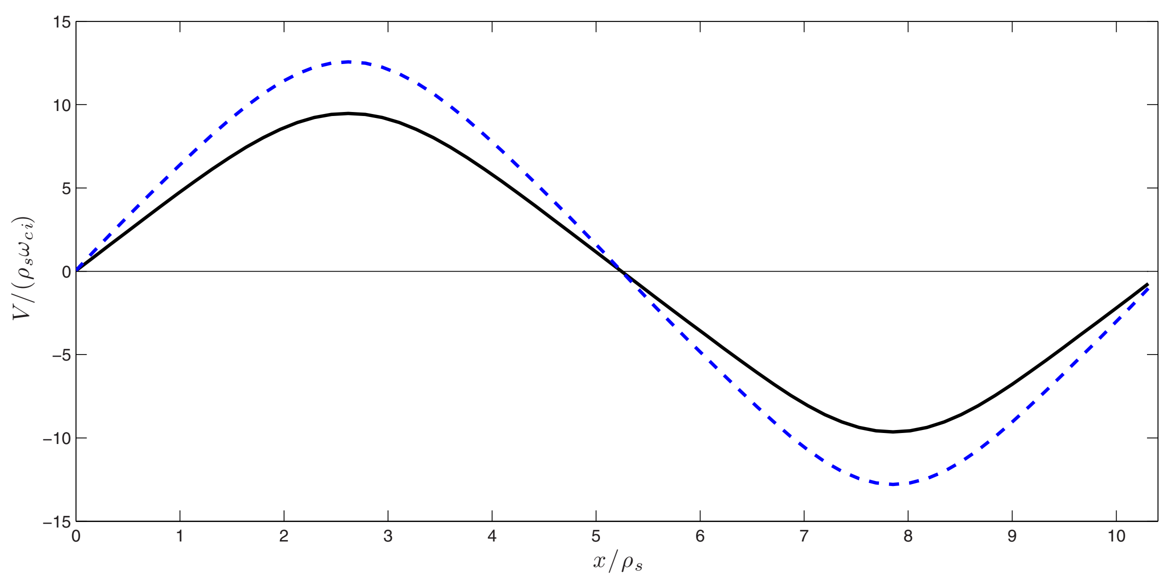

FIG. 8. (Color online) Zonal flow at equilibrium as a function of radius. Dashed line: with no collisional damping of the mean ($r_m=0$); solid line: with $r_m=10^{-4}\omega_{ci}$. The case is for $\kappa=1$, and stochastic forcing with equivalent rms velocity of $0.34\rho_s\omega_{ci}$.

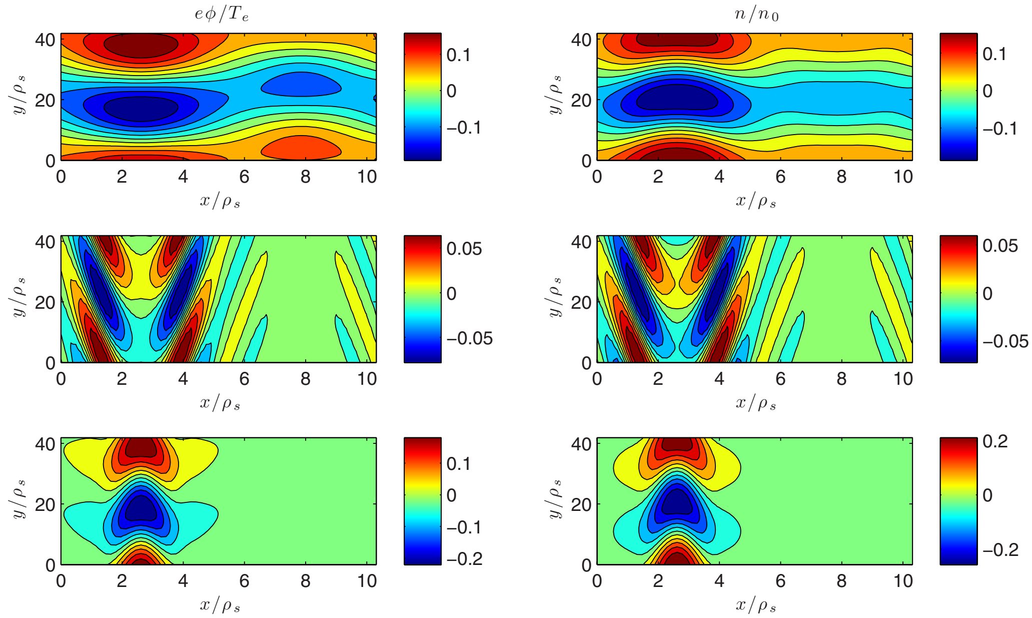

FIG. 9. (Color online) Top row: the top EOF of the eddy covariance of the component of the eddy field with poloidal wavenumber $m=1$ (on the left: perturbation electric field; on the right: perturbation density). The first EOF accounts for 32% of the total energy of the eddy field at this wavenumber. Middle row: the SO. The stochastic optimal produces 20% of the eddy energy at this wavenumber. Bottom row: the least stable eigenvalue of the operator at $m=1$. The associated growth rate is $kc_i=-0.15\omega_{ci}$. For the equilibrium zonal flow obtained at $\kappa=1$ with stochastic excitation equivalent to rms velocity of $0.34\rho_s\omega_{ci}$.

show the structure of the least damped mode and the distinct structure of the top EOF of the covariance matrix (this is the eigenfunction associated with the largest eigenvalue of $\mathbf{C}_k$) for the gravest poloidal scale $m=1$ in Figs. 9(e) and 9(f). We also show the first SO which is the structure of the excitation that would produce, if the flow was forced stochastically with this structure at unit amplitude, the highest eddy energy at statistical equilibrium (cf. for a discussion, Ref. 23). The difference in the structure of the top EOF, the least damped mode, and the SO reveal the degree of nonorthogonality of the modes of the operator which is related to their non-normality as these would be identical if the system were normal (cf. for a discussion of this point, Refs. 47 and 48).

The non-normality of the HW system is central to its dynamics. In order to appreciate its role consider the frequency spectrum of the total eddy variance resulting from excitation unbiased in time and space of the linearized HW equations. This can be obtained by Fourier transforming the perturbation equations (6a) and (6b) written in the form

$$\frac{d\hat{\psi}_k}{dt}=\mathbf{A}_k\hat{\psi}_k+\mathbf{F}\eta, \tag{24}$$

where $\mathbf{A}_k$ is given in Eq. (18), η is Gaussian white noise and $\mathbf{F}$ gives the radial structure of the forcing related to the noise covariance $\mathbf{Q}_k$ in Eq. (17) by $\mathbf{Q}_k=\mathbf{F}\mathbf{F}^\dagger$, to obtain

$$\psi_k(\omega)=\mathbf{R}_k(\omega)\mathbf{F}\hat{\eta}(\omega), \tag{25}$$

where variables that depend on ω denote the Fourier amplitudes, i.e.,

$$\hat{\psi}_k(\omega)=\frac{1}{2\pi}\int_{-\infty}^{\infty}\hat{\psi}_k(t)e^{-i\omega t}dt, \tag{26}$$

and $\hat{\eta}(\omega)$ is the Fourier amplitude of the Gaussian noise. The resolvent $\mathbf{R}(\omega)$ determines the structure of the response and is given by

$$\mathbf{R}_k(\omega)=(i\omega\mathbf{I}-\mathbf{A}_k)^{-1}. \tag{27}$$

We form the correlation matrix

$$\mathbf{C}_k(\omega)=\langle\hat{\psi}_k(\omega)\hat{\psi}_k(\omega)^\dagger\rangle=\mathbf{R}_k(\omega)\mathbf{Q}_k\mathbf{R}_k(\omega)^\dagger \tag{28}$$

and proceed to calculate the perturbation energy power spectrum as a function of phase velocity as

$$E(c)=\sum_k \text{trace}\,[\mathbf{M}_k^{1/2}\mathbf{C}_k(\omega/k)\mathbf{M}_k^{1/2}]. \tag{29}$$

Matrix $\mathbf{M}_k$ is the energy metric

$$\mathbf{M}_k=\frac{dx}{4}\begin{pmatrix}-\Delta_k & 0\\ 0 & \mathbf{I}\end{pmatrix}, \tag{30}$$

with dx the grid spacing, defined so that $E_k=\hat{\psi}_k^\dagger\mathbf{M}_k\hat{\psi}_k$ is the perturbation energy. The power spectrum is shown in Fig. 10 both for $\kappa=0$ and $\kappa=1$ along with the equivalent normal response which is obtained by calculating the power spectrum by replacing $\mathbf{A}_k$ by a diagonal matrix with elements its eigenvalues. If the forcing covariance were the identity the equivalent normal response would be given by the resonance formula,

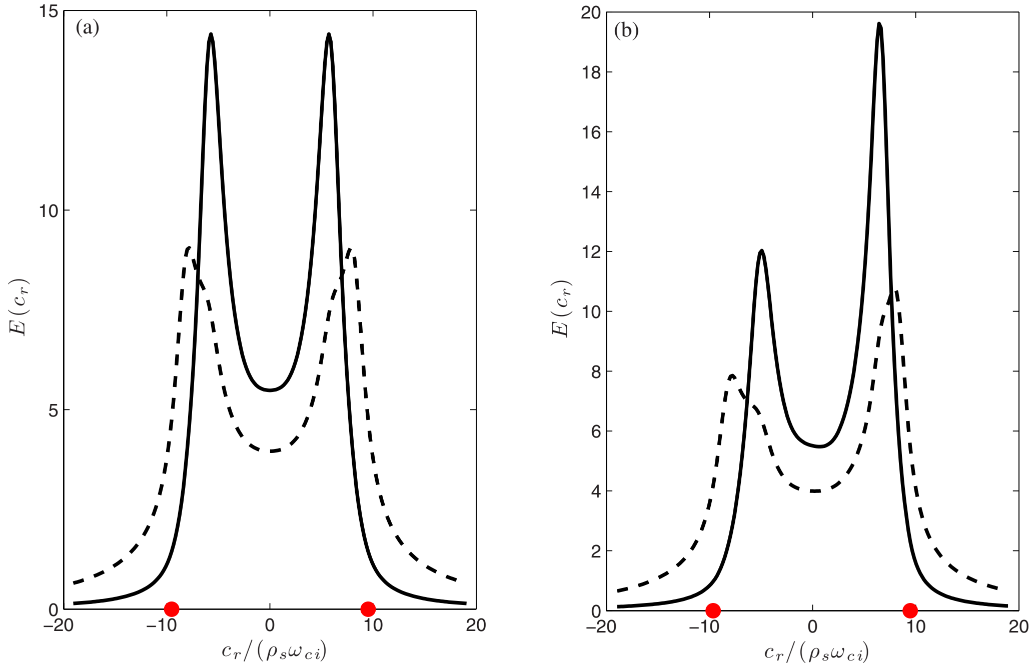

FIG. 10. (Color online) Power spectrum of the eddy energy as a function of phase speed c_r (solid line). The dashed line is the equivalent normal response and the circles mark the maximum and minimum velocities of the equilibrium flow. (a) For $\kappa=0$. (b) For $\kappa=1$. The case is for equivalent rms velocity of $0.34\rho_s\omega_{ci}$ and $r_m=10^{-4}$.

$$\sum_j \frac{1}{|i\omega - ikc_j|^2}, \tag{31}$$

where ikc_j is the jth eigenvalue of $\mathbf{A}_k$. The equivalent normal power spectrum is equal to the power spectrum when $\mathbf{A}_k$ is a normal matrix and the forcing is an identity, otherwise the power spectrum exceeds the equivalent normal power spectrum and the difference reveals the degree of non-normality. The difference reflects the excess power that is maintained by the system against friction because of the non-orthogonality of the eigenmodes.[47,48] Note that the power peaks at phase speeds near the maximum and minimum velocity of the zonal flow. An asymmetry develops as κ increases with power becoming concentrated in the prograde jet reflecting the increased instability of the prograde jet as compared with the retrograde jet when $\kappa>0$. Because the frequency response arises primarily from the gravest poloidal wavenumber this double peak in the turbulence spectrum as a function of phase speed is reflected in the frequency spectrum with a double peak at $\omega=k_{\min}\bar{v}_{\max}$, where $k_{\min}$ is the poloidal wavenumber corresponding to the gravest mode and $\bar{v}_{\max}$ is the maximum velocity of the zonal flow. Similar strongly peaked spectra indicative of coherent large scale structures in zonal jet equilibria have been observed.[49]

The particle flux at equilibrium reflects the structures producing it. This flux reaches a maximum as a function of poloidal wavenumber at $m=3$ as seen in Fig. 7(b). The flux is downgradient where the jet is prograde and becomes upgradient where the jet is retrograde. The difference between the upgradient and downgradient particle fluxes leads to a small downgradient residual which is responsible for the eddy energy source. The regions of upgradient flux show that the particle flux is produced by large coherent structures rather than resulting from random advection by small eddies as would be the case if it were diffusive.

D. Zonal flow equilibria for $\kappa>0$

The dependence of zonal flow equilibria on the amplitude of the stochastic excitation in the presence of an internal energy source ($\kappa=1$) is similar to that of zonal flows in the case without an internal energy source ($\kappa=0$). We find equilibria in the collisionless limit, $r_m=0$, and these exist for all forcing amplitudes. These equilibria are indicated by a dashed line in the bifurcation diagram in Fig. 11(c) along with the equilibria that result for $r_m=10^{-4}$. The equilibria for nonzero damping tend to the equilibria for $r_m=0$ as the stochastic excitation increases. This asymptotic is reflected in the eddy induced zonal flow acceleration which asymptotes as the stochastic excitation increases [shown in Fig. 11(b)]. The eddy kinetic energy at equilibrium increases with the amplitude of the stochastic excitation and is minimized for zero collisional damping, $r_m=0$. The particle flux, measured by the average value Γ_n/L_x, increases with stochastic excitation and for zero mean collisional damping the particle flux is increasing quadratically with stochastic excitation according to $\Gamma_n/L_x=0.0265u_{\text{rms}}^2$. From this it is clear that it would be desirable to operate a device at low stochastic excitation levels and with reduced mean collisional damping if maximizing confinement is the goal. All the equilibria of Fig. 11 are structurally stable for the chosen parameters. However, the basin of attraction of the equilibria is not the whole space. Also note that there are no equilibria with $r_m=10^{-4}$ for stochastic excitations smaller than $u_{\text{rms}}=0.065$.

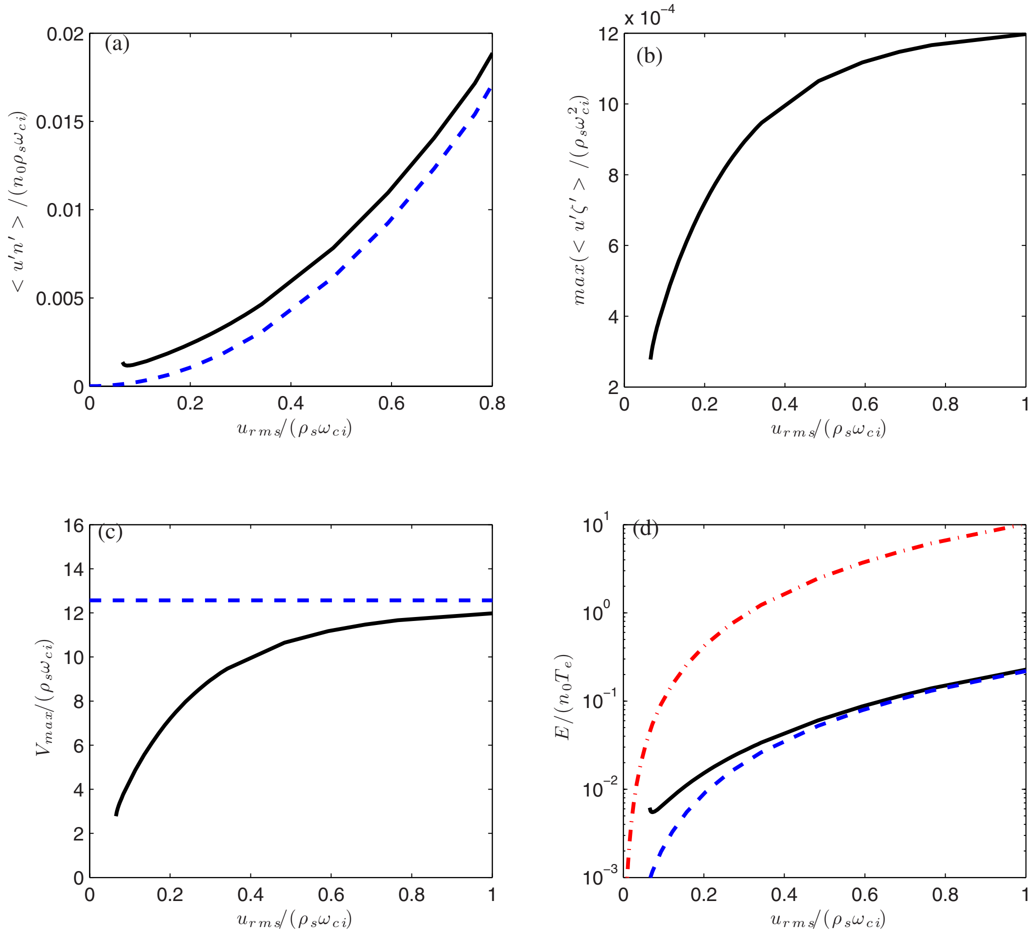

FIG. 11. (Color online) (a) Particle flux as a function of stochastic excitation measured by equivalent u_{rms}; for $r_m=10^{-4}\omega_{ci}$ (solid line) and for $r_m=0$ (dashed line). (b) Maximum vorticity flux $\langle u'\zeta'\rangle$ as a function of stochastic excitation. (c) Maximum equilibrium zonal flow velocity as a function of stochastic excitation; for $r_m=10^{-4}\omega_{ci}$ (solid line) and for $r_m=0$ (dashed line). (d) Mean eddy kinetic energy as a function of stochastic excitation. Also shown is the eddy kinetic energy maintained against dissipation in the absence of flow as a function of stochastic excitation (dash-dotted line). For $\kappa=1$.

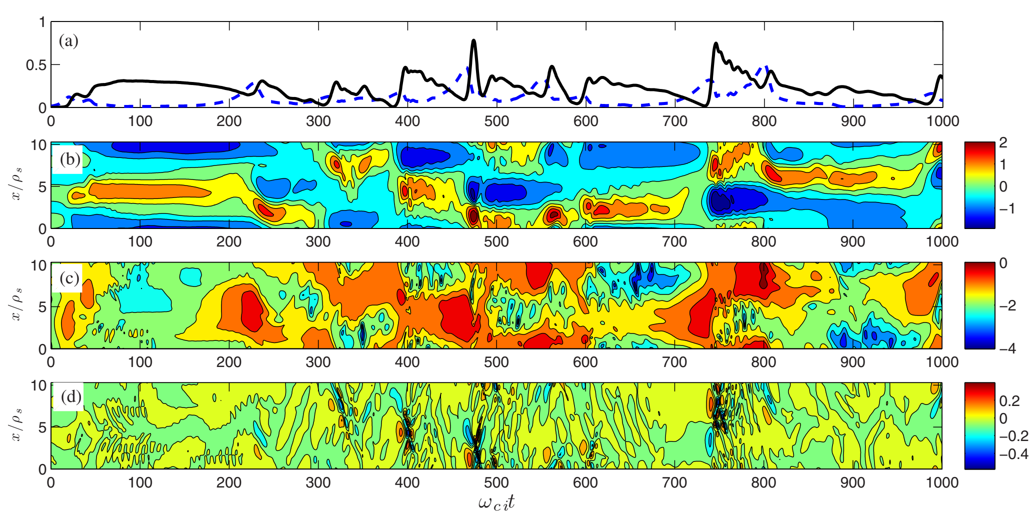

FIG. 12. (Color online) A chaotic state (analysis of perturbed trajectory differences reveals this system to be chaotic with Lyapunov exponent $0.02\omega_{ci}$). (a) Zonal flow energy (solid line), and eddy kinetic energy (dashed line) as a function of time. (b) Zonal velocity $V/(\rho_s\omega_{ci})$ as a function of radius and time. (c) Eddy kinetic energy, $\log_{10}[K_e/(n_0T_e)]$, as a function of radius and time. (d) Eddy induced zonal flow acceleration, $-\langle u'\zeta'\rangle/(\rho_s\omega_{ci}^2)$, as a function of radius and time. The parameters are $\kappa=1$, $r_m=0$ and the stochastic excitation has equivalent rms velocity of $0.34\times10^{-7}\rho_s\omega_{ci}$. For these values there exists an equilibrium zonal flow with a limited basin of attraction, and this equilibrium state cannot be approached from initial states with small zonal flows.

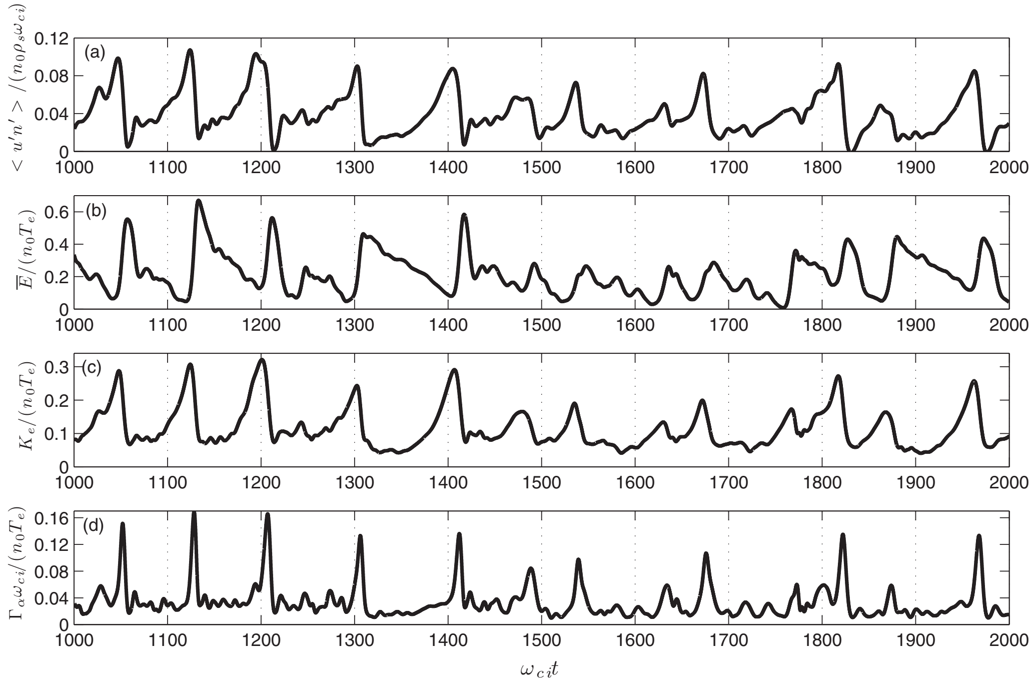

FIG. 13. For the case shown in Fig. 12: (a) particle flux at a single location as a function of time; (b) zonal flow kinetic energy; (c) eddy kinetic energy; (d) average particle flux.

Stochastic excitation, which augments the turbulence, is important for the equilibration process. In the absence of stochastic excitation the eddy field is dominated by the fastest growing modes and the structure of the covariance is not of high enough rank to include the diversity of structures required to produce equilibration. At zero or very low stochastic excitation a vacillation regime is found as occurs for slightly supercritical states in baroclinic turbulence,[50] while for sufficiently high excitation and associated turbulence levels one obtains equilibria. These equilibria for substantial stochastic excitation (i.e., $u_{\mathrm{rms}} > 0.1$) are not only structurally stable but also have a basin of attraction that spans the whole space. However, as the excitation and the supported turbulence is reduced the basin of attraction of the equilibria shrinks and finally at a critical value equilibria cease to exist. Operationally, states with low stochastic excitation and small particle fluxes can be approached by first obtaining an equilibrium by increasing the stochastic excitation and then adiabatically adjusting the parameters to reach these isolated in parameter space states.

The vacillation regime mentioned above is not a vacillation of the trajectory of a single realization of the turbulence but rather a vacillation regime in the trajectory of the probability density function of the turbulence in the (Gaussian) SSST approximation.

We show in Fig. 12 a state of chaotic DW-ZF fluctua-

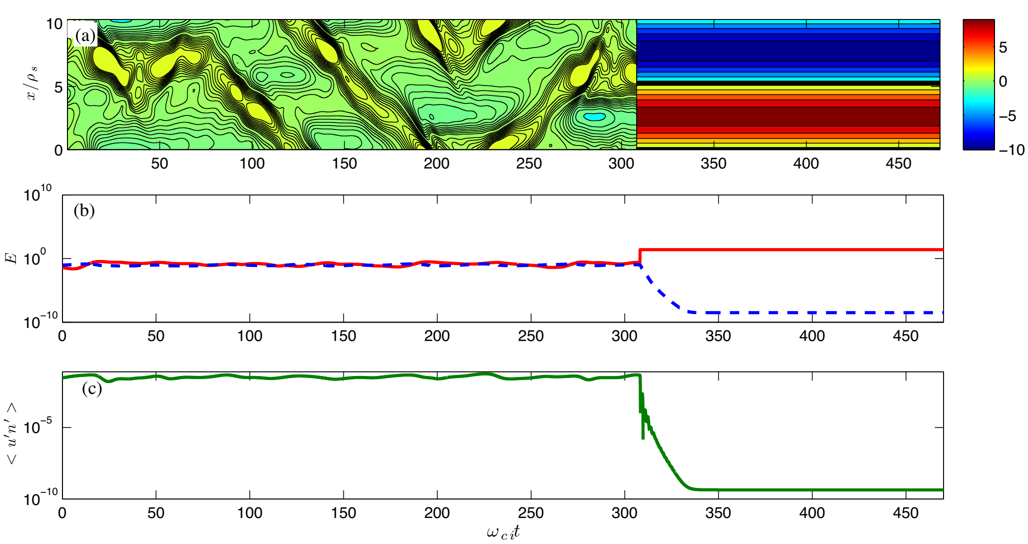

FIG. 14. (Color online) A chaotic state is laminarized by impulsive introduction of a stable zonal flow at $\omega_{ci} t = 310$. The zonal flow subsequently asymptotically approaches the equilibrium zonal flow that exists for these parameter values. (a) Zonal velocity $V/(\rho_s \omega_{ci})$ as a function of radius and time. (b) Zonal flow energy (solid line) and eddy kinetic energy (dashed line) as a function of time. (c) Mean particle flux as a function of time. For $\kappa = 1$ and $r_d = 0$.

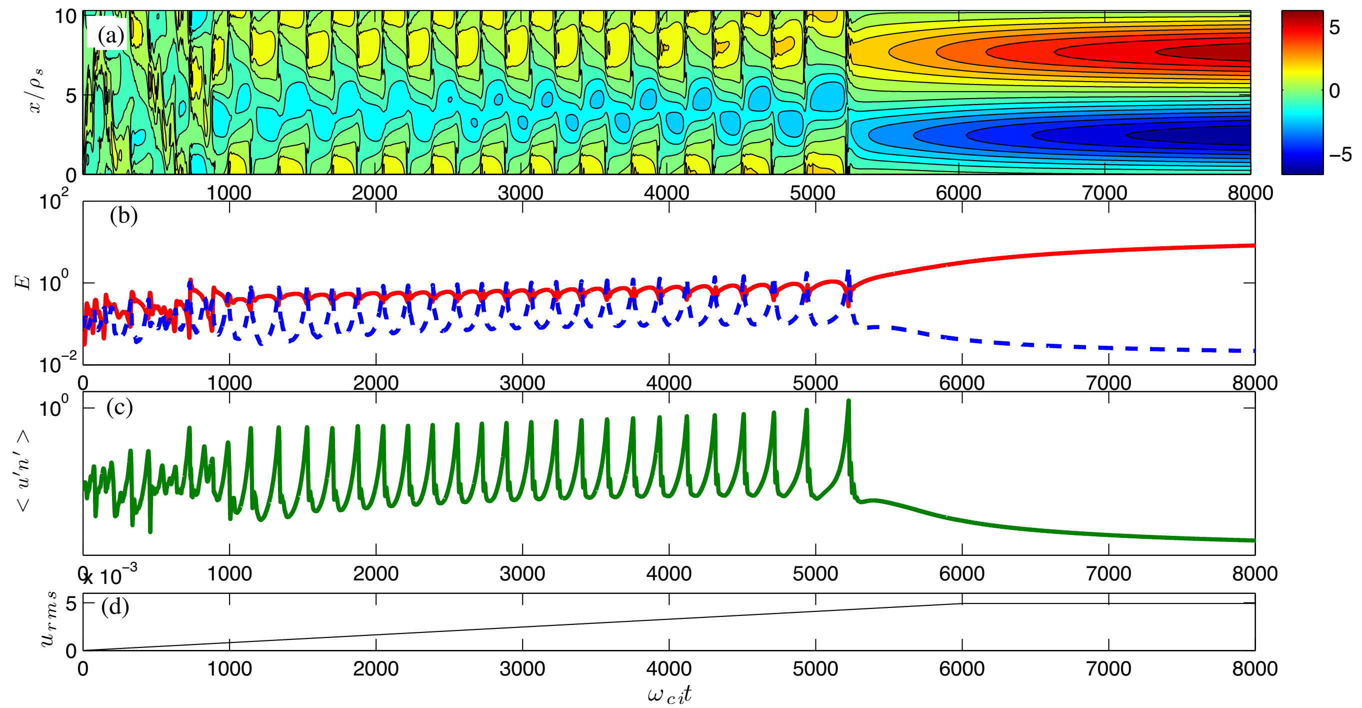

FIG. 15. (Color online) A chaotic state $(0<\omega_{ci}t<400)$ becomes quasiperiodic $(450<\omega_{ci}t<2800)$ and then settles to an equilibrium as stochastic excitation increases $(0.34\times10^{-7}\rho_s\omega_{ci}<u_{\rm rms}<0.1823\rho_s\omega_{ci})$. (a) Zonal velocity $V/(\rho_s\omega_{ci})$ as a function of radius and time. (b) Zonal flow energy (solid line) and eddy kinetic energy (dashed line) as a function of time. (c) Mean particle flux as a function of time. (d) Stochastic excitation as a function of time. For $\kappa=1$ and $r_d=0$.

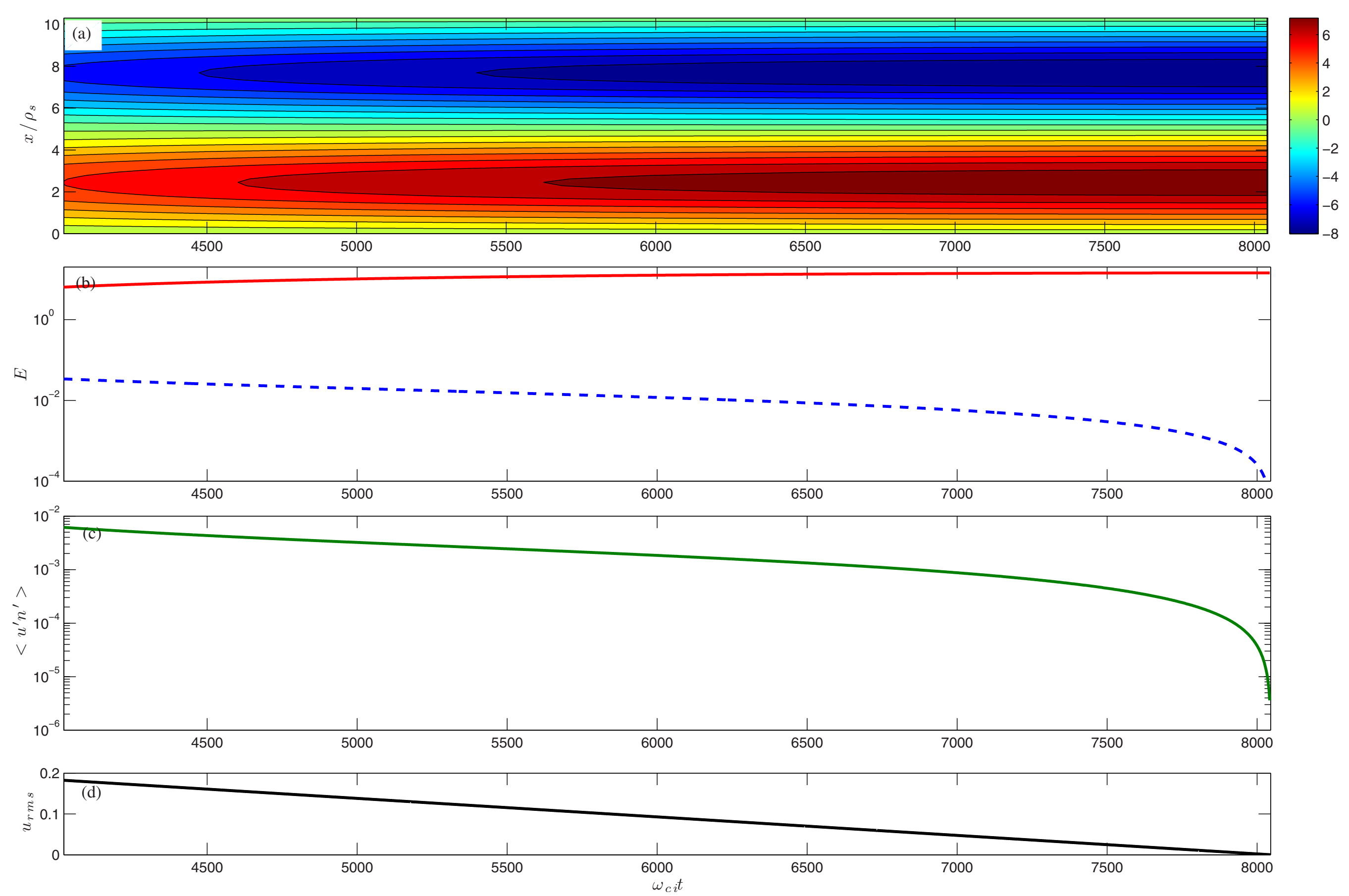

FIG. 16. (Color online) Continuation of Fig. 15. The stochastic excitation is decreased to its initial value $(u_{\rm rms}=0.34\times10^{-7}\rho_s\omega_{ci})$. The zonal flow persists while the eddy kinetic energy and the particle flux vanish with the excitation. (a) Zonal velocity $V/(\rho_s\omega_{ci})$ as a function of radius and time. (b) Zonal flow energy (solid line) and eddy kinetic energy (dashed line) as a function of time. (c) Mean particle flux as a function of time. (d) Stochastic excitation as a function of time. For $\kappa=1$ and $r_d=0$.

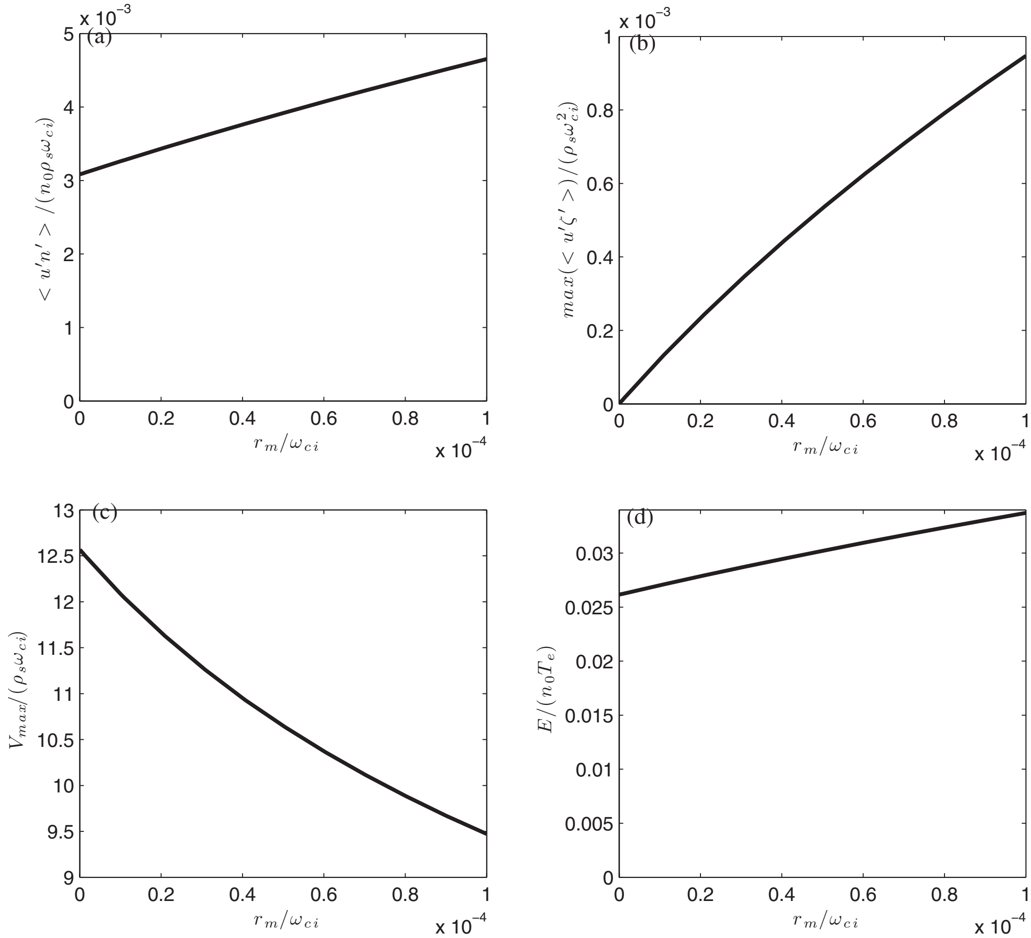

FIG. 17. Equilibrium state diagnostics as a function of mean collisional damping. (a) Particle flux. (b) Maximum vorticity flux. (c) Maximum equilibrium zonal flow velocity. (d) Mean eddy kinetic energy. The case is for $\kappa=1$, and stochastic forcing with equivalent rms velocity of $0.34\rho_s\omega_{ci}$.

tions at $\kappa=1$ with very weak forcing [producing equivalent $u_{\rm rms}=O(10^{-7})/(\rho_s\omega_{ci})$] and zero mean collisional damping. We have determined that there exists an equilibrium state but this equilibrium state has a small basin of attraction and cannot be approached from the SSST initial conditions chosen in this example (which are low turbulence levels, and very small zonal flow). A similar chaotic state persists for these parameters when the collisional damping is raised to $r_m=10^{-4}$, but for that damping there is no SSST equilibrium underlying this state [cf. Fig. 11(c)]. In Fig. 12(a) we see the initial development of the zonal flow, followed by an adjustment period, but unlike the case with strong stochastic excitation shown in Fig. 2, which adjusted to equilibrium by stabilizing the perturbations, the instability remains and alternating periods ensue of high eddy activity (low zonal flow) and low eddy activity (high zonal flow). The fluctuations settle to a chaotic bursting pattern in the zonal flow and the eddy variables as shown in Fig. 13. The eddy variables, the particle flux at a specific location, the eddy kinetic energy, and the integrated particle flux have a sawtooth structure in which a slow build up of the eddy variance associated with the underlying instability is followed by a rapid collapse of the eddy fields as the zonal flow develops and converts the eddy energy to mean zonal energy over an advective time scale. The mean zonal kinetic energy exhibits a sawtooth behavior in which the mean develops very rapidly and then slowly adjusts under the influence of the weak induced mean eddy accelerations. Such sawtooth structures have been commonly observed and simulated.[1,51]

For the same parameters that we obtained the chaotic regimes shown in Fig. 13, there exists an isolated stable equilibrium with a limited basin of attraction. This equilibrium state can be elicited by impulsively introducing any SSST zonal flow that is stable at these parameters. Immediately upon introduction of the zonal flow the eddy energy and the particle flux are quenched and the flow asymptotically relaxes to the equilibrium flow as shown in Fig. 14. If the parameters do not support an equilibrium DW-ZF state then the zonal flow eventually breaks down and a chaotic regime ensues. For example, if the collisional damping is raised to $r_m=10^{-4}\omega_{ci}$ there is no equilibrium at this amplitude of stochastic excitation and in time $O(1/r_m)$ the imposed zonal flow reverts to a chaotic state.

Regime transition can be controlled using stochastic excitation as a control parameter. As the excitation increases the chaotic bursting gives way to a quasiperiodic regime and by further increasing the stochastic excitation a fixed point DW-ZF equilibrium jet state is established as shown in Fig. 15. Having obtained an equilibrium jet state we then reduce the stochastic excitation (shown in Fig. 16) and find that the

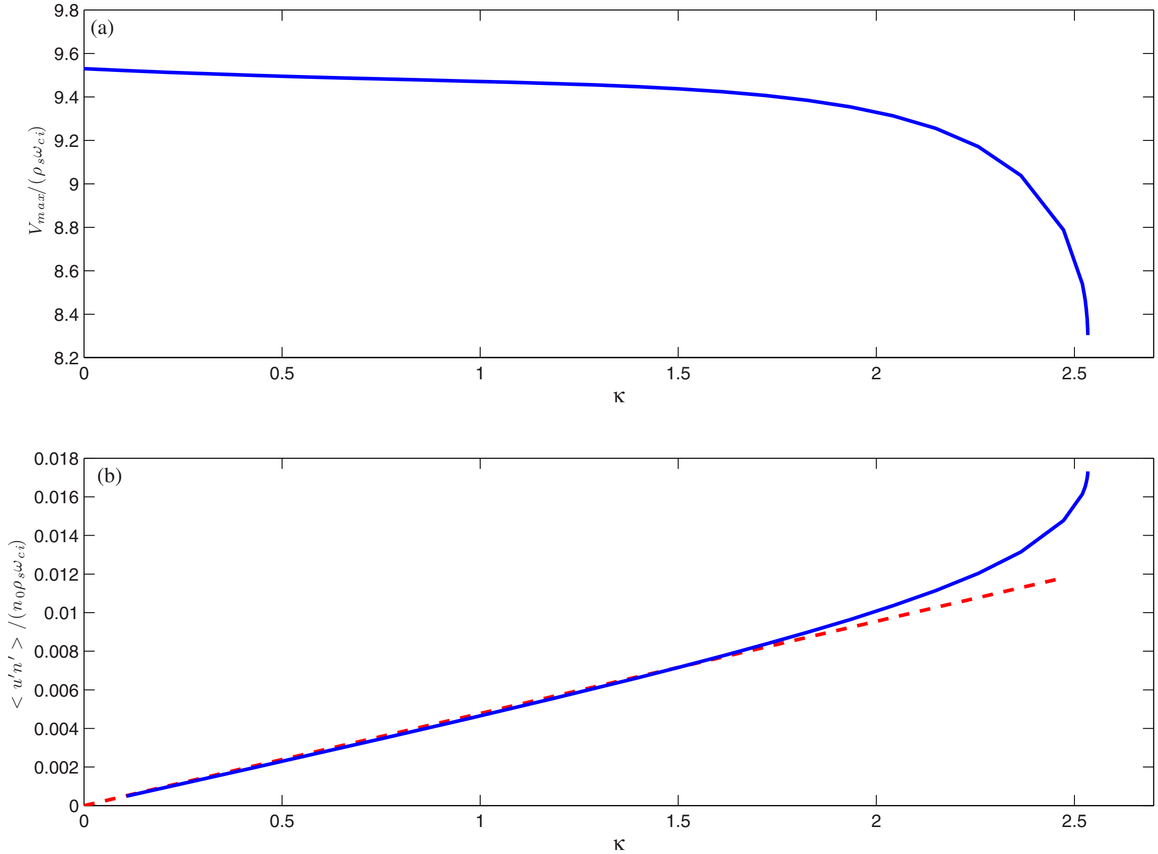

FIG. 18. (Color online) Equilibrium state diagnostics as a function of density gradient κ. (a) Maximum velocity of the equilibrium zonal flow. (b) The mean particle flux (solid line). The mean particle flux increases at first linearly as $0.05\kappa/Lx$ (dashed line). The parameters are $r_m=10^{-4}$ and the stochastic excitation supports equivalent rms velocity of $0.34\rho_s\omega_{ci}$.

jet persists as the stochastic excitation is reduced and both the eddy kinetic energy and the particle flux vanish with the excitation. This equilibrium state exists at the same parameter values for which periodic and chaotic behaviors are obtained. Hysteretic transition between a steady zonal flow state and a chaotic turbulent state is common in turbulent systems such as sheared boundary layer flows which exist in laminar and turbulent states at the same parameter values.

Dependence of zonal flow, eddy variances, and fluxes at equilibrium on mean collisional damping is shown Fig. 17; the particle flux increases with mean collisional damping, as does the eddy energy while the zonal flow velocity decreases, as is also found in turbulence simulations.[14]

E. Loss of structural stability at large κ

We now investigate zonal flow equilibria as a function of κ. These equilibria, as already discussed, are most easily initialized at high stochastic excitation amplitude and low mean collisional damping. We study the dependence of these equilibria on κ at high turbulence levels [with equivalent $u_{\rm rms}=0.34/(\rho_s\omega_{ci})$]. The maximum zonal flow speed is shown in Fig. 18(a) as a function of κ and the mean particle flux averaged over the whole domain is shown in Fig. 18(b). The particle flux is seen to initially increase linearly with κ. The equilibria are globally attracting up to about $\kappa=1.5$, for the parameters of this problem, but the basin of attraction contracts as κ is increased until the flow becomes structurally unstable at $\kappa=2.534$, and no equilibria exist for larger values of κ. Although equilibria exist for $\kappa>1.5$ these equilibria cannot be reached from the above listed fixed parameters starting from any initial condition, but they can be reached by first establishing an equilibrated state at a lower value of κ and then increasing κ adiabatically; although operationally these states are most readily established by first going to higher stochastic excitation, corresponding to a higher level of turbulence, then increasing κ and finally reducing the excitation.

The equilibrated flows and the corresponding minimum damping decay rate of the least damped mode at each poloidal wavenumber m are shown in Fig. 19 for the critical $\kappa_c=2.534$ and for the smaller unstable stratifications $\kappa=2.52$ and $\kappa=2.0425$. As the critical value of κ_c is approached the poloidal, $m=5$ wave, tends toward instability. However, as $\kappa\to\kappa_c$ the damping decay rate of the least damped mode approaches, for the chosen parameters $kc_{i\max}\to-0.12\omega_{ci}$ while the fluxes and the equilibrium zonal flow tend to diverge as κ_c is approached and no equilibrium flows can be sustained for $\kappa>\kappa_c$ and transition to a time varying state occurs. This result shows that the jet first loses structural stability as a function of κ rather than modal stability.

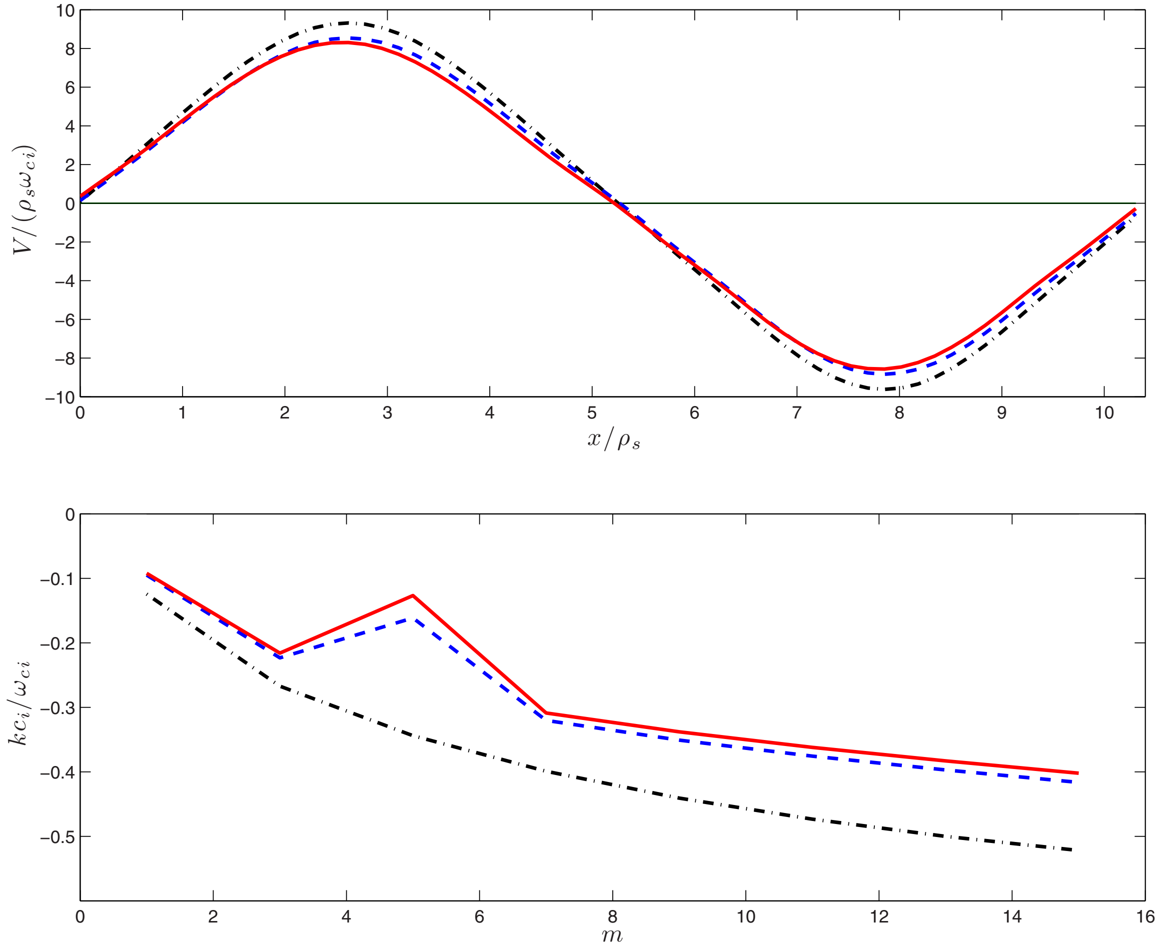

FIG. 19. (Color online) Approach to structural instability as a function of κ. Top: zonal flow velocities as the critical $\kappa_c=2.534$ is approached. Bottom: the corresponding maximum growth rate of perturbations as a function of poloidal wavenumber m. Solid line: $\kappa=2.534$; dashed line: $\kappa=2.52$; dash-dotted line: for $\kappa=2.0425$. The parameters are $r_m=10^{-4}$ and the stochastic excitation has equivalent rms velocity of $0.34\rho_s\omega_{ci}$.

IV. DISCUSSION

There are a number of points we wish to emphasize in connection with the above results.

(1) A novel concept arising from SSST is that of the structural stability boundary for zonal flow breakdown as distinct from breakdown related to shear instability of the zonal flow.
(2) Multiple DW-ZF regimes are predicted to exist in parameter space including a regime of steady zonal flows as well as regimes of periodic, quasiperiodic, and chaotic bursting or "sawtooth" behavior. These regimes provide opportunity for placing and manipulating confinement devices to be in a desired dynamical state between high and low confinements.
(3) SSST predicts that isolated DW-ZF equilibria at high κ are not connected continuously to lower κ states but that these states can be reached either using external turbulence excitation or finite amplitude state perturbation to promote the system between these equilibria.
(4) A mechanism for introducing and modulating turbulence levels is predicted to provide a powerful control parameter for placing the DW-ZF system in desired confinement states.
(5) In the limit of vanishing zonal flow collisional damping a universal DW-ZF state is supported in which a precise balance between downgradient momentum transport by small wavenumbers and upgradient transport by high poloidal wavenumbers occurs. This asymptotic equilibrium predicts that band limiting turbulence can prevent formation of stable equilibrium zonal flows.
(6) Density fluxes are not diffusive but rather are primarily produced by large scale structures. Robust fluxes both up and down the mean gradient occur, and it follows that particle transport analysis requires a full wave solution.

V. CONCLUSION

Emergence of zonal jets in turbulent flow and the relation of these jets to the statistical equilibrium of the turbulent state is a problem of great theoretical and practical interest. This problem is particularly compelling in the case of turbulent plasmas because of the relationship of zonal jets to the H states that limit turbulent transport of particles and heat in magnetic confinement fusion devices. DW-ZF interaction dynamics is responsible for the generation and regulation of these zonal flows so it follows that prospects for predicting and controlling the H state require improvement in fundamental understanding of the mechanism underlying the statistical steady state of zonal jets in drift wave turbulence. In this work we applied the methods of SSST to the HW model to study the emergence, stability, and effect on transport of zonal jets in the DW-ZF system. We find robust zonal jet formation in agreement with both experiment and simulation and obtain parameter requirements for jet formation and breakdown. We find multiple regimes including chaotic, periodic, and steady and show that externally imposed turbulence and finite amplitude zonal flow perturbations can be used to control regime transition. We find suppression of particle transport by zonal flows and show that this transport is not diffusive in nature. These results provide a basis for predicting and controlling confinement regimes in DW-ZF turbulence.

ACKNOWLEDGMENTS

Discussions with S. Nazarenko and B. Nadiga are gratefully acknowledged. This work was supported by NSF Grant No. ATM-0123389.

[1] P. H. Diamond, S.-I. Itoh, K. Itoh, and T. S. Hahm, Plasma Phys. Controlled Fusion **47**, R35 (2005).
[2] A. P. Ingersoll, Science **248**, 308 (1990).
[3] A. M. Balk, S. V. Nazarenko, and V. E. Zakharov, Phys. Lett. A **146**, 217 (1990).
[4] R. L. Panetta, J. Atmos. Sci. **50**, 2073 (1993).
[5] G. K. Vallis and M. E. Maltrud, J. Phys. Oceanogr. **23**, 1346 (1993).
[6] J. Y.-K. Cho and L. M. Polvani, Science **273**, 335 (1996).
[7] H.-P. Huang and W. A. Robinson, J. Atmos. Sci. **55**, 611 (1998).
[8] B. F. Farrell and P. J. Ioannou, J. Atmos. Sci. **60**, 2101 (2003).
[9] B. F. Farrell and P. J. Ioannou, J. Atmos. Sci. **64**, 3652 (2007).
[10] C. Connaughton, B. Nadiga, S. Nazarenko, and B. Quinn, e-print arXiv:0905.2243.
[11] R. Krishnamurti and L. N. Howard, Proc. Natl. Acad. Sci. U.S.A. **78**, 1981 (1981).
[12] A. Fujisawa, K. Itoh, A. Shimizu, H. Nakano, S. Ohshima, H. Iguchi, K. Matsuoka, S. Okamura, T. Minami, Y. Yoshimura, K. Nagaoka, K. Ida, K. Toi, C. Takahashi, M. Kojima, S. Nishimura, M. Isobe, C. Suzuki, T. Akiyama, T. Ido, Y. Nagashima, S.-I. Itoh, and P. H. Diamond, Phys. Plasmas **15**, 055906 (2008).
[13] A. Fujisawa, A. Shimizu, H. Nakano, S. Ohshima, K. Itoh, Y. Nagashima, S.-I. Itoh, H. Iguchi, Y. Yoshimura, T. Minami, K. Nagaoka, C. Takahashi, M. Kojima, S. Nishimura, M. Isobe, C. Suzuki, T. Akiyama, T. Ido, K. Matsuoka, S. Okamura, and P. H. Diamond, J. Phys. Soc. Jpn. **76**, 033501 (2007).
[14] K. Itoh, S. Toda, A. Fujisawa, S. Itoh, and S. Yagi, Phys. Plasmas **14**, 020702 (2007).
[15] P. L. Read, Y. H. Yamazaki, S. R. Lewis, P. D. Williams, R. Wordsworth, and K. Miki-Yamazaki, J. Atmos. Sci. **64**, 4031 (2007).
[16] E. Mazzucato, S. Batha, M. Beer, and M. Bell, Phys. Rev. Lett. **77**, 3145 (1996).
[17] C. Holland, J. H. Yu, A. James, D. Nishijima, M. Shimada, N. Taheri, and G. R. Tynan, Phys. Rev. Lett. **96**, 195002 (2006).
[18] T. Nozawa and Y. Yoden, Phys. Fluids **9**, 2081 (1997).
[19] A. P. Ingersoll, T. Dowling, P. J. Gierasch, G. Orton, P. L. Read, A. Sanchez-Lavega, A. Showman, A. A. Simon-Miller, and A. R. Vasavada, in *Jupiter: The Planet, Satellites, and Magnetosphere*, edited by F. Bagenal, T. E. Dowling, and W. B. McKinnon (Cambridge University Press, Cambridge, 2004), pp. 105–128.
[20] C. Salyk, A. P. Ingersoll, J. Lorre, A. Vasavada, and A. D. Del Genio, Icarus **185**, 430 (2006).
[21] Y. Kitamura and K. Ishioka, J. Atmos. Sci. **64**, 3340 (2007).
[22] B. F. Farrell and P. J. Ioannou, J. Atmos. Sci. **50**, 4044 (1993).
[23] B. F. Farrell and P. J. Ioannou, J. Atmos. Sci. **53**, 2025 (1996).
[24] T. DelSole and B. F. Farrell, J. Atmos. Sci. **53**, 1781 (1996).
[25] M. Newman, P. D. Sardeshmukh, and C. Penland, J. Atmos. Sci. **54**, 435 (1997).
[26] Y. Zhang and I. M. Held, J. Atmos. Sci. **56**, 3416 (1999).
[27] T. DelSole, Surv. Geophys. **25**, 107 (2004).
[28] B. F. Farrell and P. J. Ioannou, J. Atmos. Sci. **65**, 3353 (2008).
[29] B. F. Farrell and P. J. Ioannou, J. Atmos. Sci. **66**, 3197 (2009).
[30] B. F. Farrell and P. J. Ioannou, J. Atmos. Sci. **66**, 2444 (2009).
[31] R. Sánchez, D. E. Newman, J.-N. Leboeuf, B. A. Carreras, and V. K. Decyk, Phys. Plasmas **16**, 055905 (2009).
[32] M. Shats, K. Toi, K. Ohkuni, and Y. Yoshimura, Phys. Rev. Lett. **84**, 6042 (2000).
[33] W. J. T. Bos, S. Futatani, S. Benkadda, M. Farge, and K. Schneider, Phys. Plasmas **15**, 072305 (2008).
[34] P. J. Ioannou and R. S. Lindzen, J. Atmos. Sci. **43**, 2999 (1986).
[35] I. N. James, J. Atmos. Sci. **44**, 3710 (1987).
[36] H. H. Roe and R. S. Lindzen, J. Atmos. Sci. **53**, 2749 (1996).
[37] R. Numata, R. Ball, and R. L. Dewar, Phys. Plasmas **14**, 102312 (2007).
[38] A. Hasegawa and A. Mima, Phys. Fluids **21**, 87 (1978).
[39] B. F. Farrell and P. J. Ioannou, Phys. Fluids A **5**, 2600 (1993).
[40] B. F. Farrell and P. J. Ioannou, J. Atmos. Sci. **51**, 2685 (1994).
[41] B. F. Farrell and P. J. Ioannou, J. Atmos. Sci. **52**, 1642 (1995).
[42] T. DelSole, J. Atmos. Sci. **53**, 1617 (1996).
[43] J. S. Whitaker and P. D. Sardeshmukh, J. Atmos. Sci. **55**, 237 (1998).
[44] T. DelSole, J. Atmos. Sci. **58**, 3762 (2001).
[45] B. F. Farrell and P. J. Ioannou, J. Atmos. Sci. **50**, 200 (1993).
[46] Z. Lin, T. Hahm, W. Lee, W. Tang, and R. White, Phys. Plasmas **7**, 1857 (2000).
[47] B. F. Farrell and P. J. Ioannou, Phys. Rev. Lett. **72**, 1188 (1994).
[48] P. J. Ioannou, J. Atmos. Sci. **52**, 1155 (1995).
[49] C. E. Bush, M. G. Bell, R. E. Bell, J. Boedo, E. D. Fredrickson, S. M. Kaye, S. Kubota, B. P. LeBlanc, R. Maingi, R. J. Maqueda, S. A. Sabbagh, V. A. Soukhanovskii, D. Stutman, D. W. Swain, J. B. Wilgren, S. J. Zweben, W. M. Davis, D. A. Gates, D. W. Johnson, R. Kaita, H. W. Kugel, K. C. Lee, D. Mastrovito, S. Medley, J. E. Menard, D. Mueller, M. Ono, F. Paoletti, H. Park, S. J. Paul, Y.-K. M. Peng, R. Raman, P. G. Roney, A. L. Roquemore, C. H. Skinner, E. J. Synakowski, G. Taylor, and the NSTX Team, Phys. Plasmas **10**, 1755 (2003).
[50] J. Pedlosky, J. Atmos. Sci. **34**, 1898 (1977).
[51] F. Wagner, Plasma Phys. Controlled Fusion **49**, B1 (2007).